TRANSPARENT
PROCESS

THE
EMBO
JOURNAL

m⁶A-mediated alternative splicing coupled with nonsense-mediated mRNA decay regulates SAM synthetase homeostasis

Eichi Watabe[1], Marina Togo-Ohno[1], Yuma Ishigami[2] (iD), Shotaro Wani[1], Keiko Hirota[3,†], Mariko Kimura-Asami[1,‡], Sharmin Hasan[1] (iD), Satomi Takei[1], Akiyoshi Fukamizu[3], Yutaka Suzuki[4], Tsutomu Suzuki[2] (iD) & Hidehito Kuroyanagi[1,5,*] (iD)

Abstract

Alternative splicing of pre-mRNAs can regulate gene expression levels by coupling with nonsense-mediated mRNA decay (NMD). In order to elucidate a repertoire of mRNAs regulated by alternative splicing coupled with NMD (AS-NMD) in an organism, we performed long-read RNA sequencing of poly(A)⁺ RNAs from an NMD-deficient mutant strain of *Caenorhabditis elegans*, and obtained full-length sequences for mRNA isoforms from 259 high-confidence AS-NMD genes. Among them are the S-adenosyl-L-methionine (SAM) synthetase (*sams*) genes *sams-3* and *sams-4*. SAM synthetase activity autoregulates *sams* gene expression through AS-NMD in a negative feedback loop. We furthermore find that METT-10, the orthologue of human U6 snRNA methyltransferase METTL16, is required for the splicing regulation *in vivo*, and specifically methylates the invariant AG dinucleotide at the distal 3′ splice site (3′SS) *in vitro*. Direct RNA sequencing coupled with machine learning confirms m⁶A modification of endogenous *sams* mRNAs. Overall, these results indicate that homeostasis of SAM synthetase in *C. elegans* is maintained by alternative splicing regulation through m⁶A modification at the 3′SS of the *sams* genes.

Introduction

Alternative splicing of precursor messenger RNAs (pre-mRNAs) contributes not only to proteome diversity (Nilsen & Graveley, 2010; Ule & Blencowe, 2019) but also to regulation of gene expression levels by generating mRNA isoforms with a premature termination codon (PTC) (Hamid & Makeyev, 2014; Sibley, 2014). Such unproductively spliced mRNAs are unstable and almost undetectable due to an mRNA surveillance system termed nonsense-mediated mRNA decay (NMD) (Lareau & Brenner, 2015; Kishor *et al*, 2019; Kurosaki *et al*, 2019). Genetic studies in yeast and nematode identified evolutionarily conserved NMD factors including UPF1, UPF2, and UPF3 (Pulak & Anderson, 1993; He & Jacobson, 1995). Searches for mRNAs stabilized under NMD-deficient conditions in a variety of organisms identified many splicing variants as natural NMD substrates in addition to mRNAs from snoRNA host genes, pseudogenes, long noncoding genes, and viral genes (Chapin *et al*, 2014; Kawashima *et al*, 2014; Celik *et al*, 2017; Colombo *et al*, 2017; Muir *et al*, 2018). Among the genes whose expression is regulated through alternative splicing coupled with NMD (AS-NMD), many splicing factors and regulators have been shown to negatively autoregulate their own expression at the level of pre-mRNA splicing (Jumaa & Nielsen, 1997; Lejeune *et al*, 2001; Sureau *et al*, 2001; Lareau *et al*, 2007; Ni *et al*, 2007; McGlincy *et al*, 2010; Turunen *et al*, 2013; Jangi *et al*, 2014; Sun *et al*, 2017).

An advantage of utilizing *C. elegans* as a model organism for studying AS-NMD is in that its NMD factors are not essential for the development or fertility, allowing for genetic studies and genome-wide survey of natural NMD substrates *in vivo*. The *C. elegans* genome is rich in introns like those of higher organisms (Consortium CeS, 1998), and > 25% of its protein-coding genes undergo alternative pre-mRNA splicing (Ramani *et al*, 2009; Ramani *et al*,

1   Laboratory of Gene Expression, Medical Research Institute, Tokyo Medical and Dental University (TMDU), Bunkyo-ku, Tokyo, Japan
2   Department of Chemistry and Biotechnology, Graduate School of Engineering, University of Tokyo, Bunkyo-ku, Tokyo, Japan
3   Life Science Center for Survival Dynamics, Tsukuba Advanced Research Alliance (TARA), University of Tsukuba, Tsukuba-shi, Ibaraki, Japan
4   Department of Computational Biology and Medical Sciences, Graduate School of Frontier Sciences, University of Tokyo, Kashiwa-shi, Chiba, Japan
5   Department of Biochemistry, Graduate School of Medicine, University of the Ryukyus, Nishihara-cho, Okinawa, Japan
    *Corresponding author. Tel: +81 98 895 1112; E-mail: hidehito@med.u-ryukyu.ac.jp
    †Present address: Department of Hygiene and Public Health, School of Medicine, Tokyo Women's Medical University, Shinjuku-ku, Tokyo, Japan
    ‡Present address: Center for Preventive Medicine, St. Luke's International Hospital Affiliated Clinic, St. Luke's International University, Chuo-ku, Tokyo, Japan

2011; Tourasse *et al*, 2017). Early studies with splicing-sensitive microarrays identified 30 genes regulated by AS-NMD, including those for splicing regulators (Barberan-Soler & Zahler, 2008; Barberan-Soler *et al*, 2009). We previously reported RNA-seq analysis of mRNAs in an NMD-deficient mutant *smg-2* and demonstrated that eight of ribosomal protein genes undergo negative autoregulation through AS-NMD (Takei *et al*, 2016). Recently, AS-NMD has been demonstrated to play crucial roles in longevity of long-lived mutants or by dietary restriction and RNA-seq analyses identified alternative splicing events relevant to longevity (Son *et al*, 2017; Tabrez *et al*, 2017). A caveat of the RNA-seq analyses, however, is that an entire sequence of each mRNA molecule cannot be accurately reconstructed from the short-read RNA-seq data.

Post-transcriptional base modification of mRNAs has emerged as a new layer of regulatory mechanisms controlling gene expression (Frye *et al*, 2016). Among such modifications, N^6-methyladenosine (m^6A) is the most prevalent internal modification in mRNAs in higher eukaryotic species (Wei *et al*, 1975). The m^6A modification is reversible; methyltransferases ("writers") and demethylases ("erasers") methylate and demethylate mRNAs, respectively (Duan *et al*, 2019; Shi *et al*, 2019; Zaccara *et al*, 2019; Huang *et al*, 2020a; Huang *et al*, 2020b). Almost all of m^6A modifications in mRNAs are deposited by a multicomponent m^6A methyltransferase complex composed of a core component, the methyltransferase-like 3 (METTL3)/METTL14 heterodimer, and other regulatory factors (Liu *et al*, 2014; Ping *et al*, 2014; Schwartz *et al*, 2014). The m^6A modifications may alter local RNA structures to switch interaction with RNA-binding proteins (Liu *et al*, 2015) or may affect splicing, nuclear export, translation initiation, and stability of mRNAs through specific recognition by m^6A-binding proteins ("readers") such as YTHDC1, YTHDF1, and YTHDF2 (Wang *et al*, 2015; Xiao *et al*, 2016; Roundtree *et al*, 2017). The m^6A modifications in RNAs can be removed by erasers FTO and ALKBH5 (Jia *et al*, 2011; Zheng *et al*, 2013). In *C. elegans*, however, orthologous genes for the m^6A writers, erasers, and readers mentioned above are absent from the genome (Cunningham *et al*, 2019; Arribere *et al*, 2020) and recent studies demonstrated that only a limited fraction of mRNAs would have m^6A modification (van Delft *et al*, 2017; Liberman *et al*, 2020). It is therefore still unclear whether the m^6A modification also plays regulatory roles in mRNA metabolism in *C. elegans*.

In this study, we performed high-throughput long-read sequencing of mRNAs to reveal their full-length sequences in an NMD-deficient mutant strain with a mutation in the *smg-2* gene, encoding the crucial NMD factor UPF1. We summarize features of genes subjected to AS-NMD. To search for a novel regulatory mechanism of AS-NMD other than autoregulation by RNA-binding proteins, we focused on *S*-adenosyl-L-methionine (SAM) synthetase genes and demonstrate that m^6A modification at the invariant AG dinucleotide of a 3′ splice site (SS) by a methyltransferase METT-10 switches the choice of competing 3′SSs, leading to AS-NMD for homeostasis of the enzyme.

Results

Full-length sequences of NMD isoforms in *C. elegans*

In order to reveal full-length sequences of natural NMD substrates in *C. elegans*, we performed long-read sequencing of poly(A)$^+$ RNAs from the *smg-2 (yb979)* mutant (Kuroyanagi *et al*, 2007) with a direct RNA sequencing protocol on a Nanopore MinION platform (Garalde *et al*, 2018). To minimize over representation of abundant mRNAs from housekeeping genes, we purified newly synthesized RNAs after 6-h metabolic labeling with 4-thiouracil (4TU) in synchronized L1 larvae and directly sequenced the nascent poly(A)$^+$ RNAs (see Methods). After base-calling, 1,402,229 reads were mapped to the *C. elegans* genome and we identified 12,517 mRNA isoforms from 8,028 genes (Dataset EV1) supported by at least 3 reads whose exon-exon junctions were also supported by short-read RNA-seq data from *smg-2* mutants in previous studies (Kuroyanagi *et al*, 2013; Takei *et al*, 2016; Son *et al*, 2017). For comparison, we collected and pooled as many direct RNA sequencing data in a public database as possible for mRNAs from various stages of a wild-type strain N2 (Roach *et al*, 2020). With the same procedure, 3,511,592 reads were mapped to the genome and 18,376 isoforms from 11,331 genes (Dataset EV1) were supported by short-read RNA-seq data from N2 in previous studies (Takei *et al*, 2016; Son *et al*, 2017). Figure 1A summarizes numbers of exon-exon junctions identified in the *smg-2* mutant and/or N2 as well as those deduced from gene models in WormBase (WS271) in 6,642 genes commonly detected in the two strains. Even though the number of reads and the stage of the worms are limited in our analysis, we detected more than 700 novel junctions that were not detected in N2 or predicted in WormBase (Fig 1A), suggesting that mRNAs with unusual splicing patterns are stabilized in the *smg-2* mutant.

In order to identify mRNA isoforms whose proportions to the total mRNAs within the genes are significantly different between the *smg-2* mutant and N2, we performed Fisher's exact tests with read numbers in the Nanopore sequencing data for 2,931 genes with two or more isoforms and with at least 10 total reads in each strain (Dataset EV1). Here, we assumed that the proportions of the NMD

Figure 1. Long-read sequencing reveals putative NMD isoforms enriched in the *smg-2* mutant.

A   Venn diagram of exon-exon junctions in 6,642 common genes identified among the Nanopore reads from the *smg-2 (yb979)* mutant and wild-type N2 as well as those deduced from gene models in WormBase (WS271).

B   Volcano plot of 8,701 mRNA isoforms from 2,931 genes with multiple isoforms. X-axis indicates a difference in percentage of each mRNA isoform within the gene ($\Delta\%_{smg-2-N2}$). Y-axis indicates $-\log_{10}$ of *P*-value in Fisher's exact tests. Blue symbols indicate 219 mRNA isoforms significantly depleted from the *smg-2* mutant ($P < 0.05$, $\Delta\%_{smg-2-N2} < -10$). Red symbols indicate 420 isoforms significantly enriched in the *smg-2* mutant ($P < 0.05$, $\Delta\%_{smg-2-N2} > 10$).

C, D   Length distribution of 3′UTRs (C) and proportions of putative PTC-containing isoforms (D) in 10,136 mRNA isoforms detected in N2 and/or *smg-2* (All), the 219 isoforms depleted from and the 420 isoforms enriched in the *smg-2* mutant.

E   GO terms significantly enriched in 259 genes with *smg-2*-enriched PTC isoforms (top) and in 30 genes with *smg-2*-depleted PTC isoforms (bottom). Modified Fisher's exact *P*-values in the DAVID Bioinformatics system are indicated. Note that 14 of the 30 genes with the *smg-2*-depleted mRNA PTC isoforms are common with those having *smg-2*-enriched PTC isoforms. This is why the same GO terms are enriched in these two groups. The mRNAs from such genes likely contain upstream open reading frames (uORFs), which may not be directly involved in or differentially affect NMD.
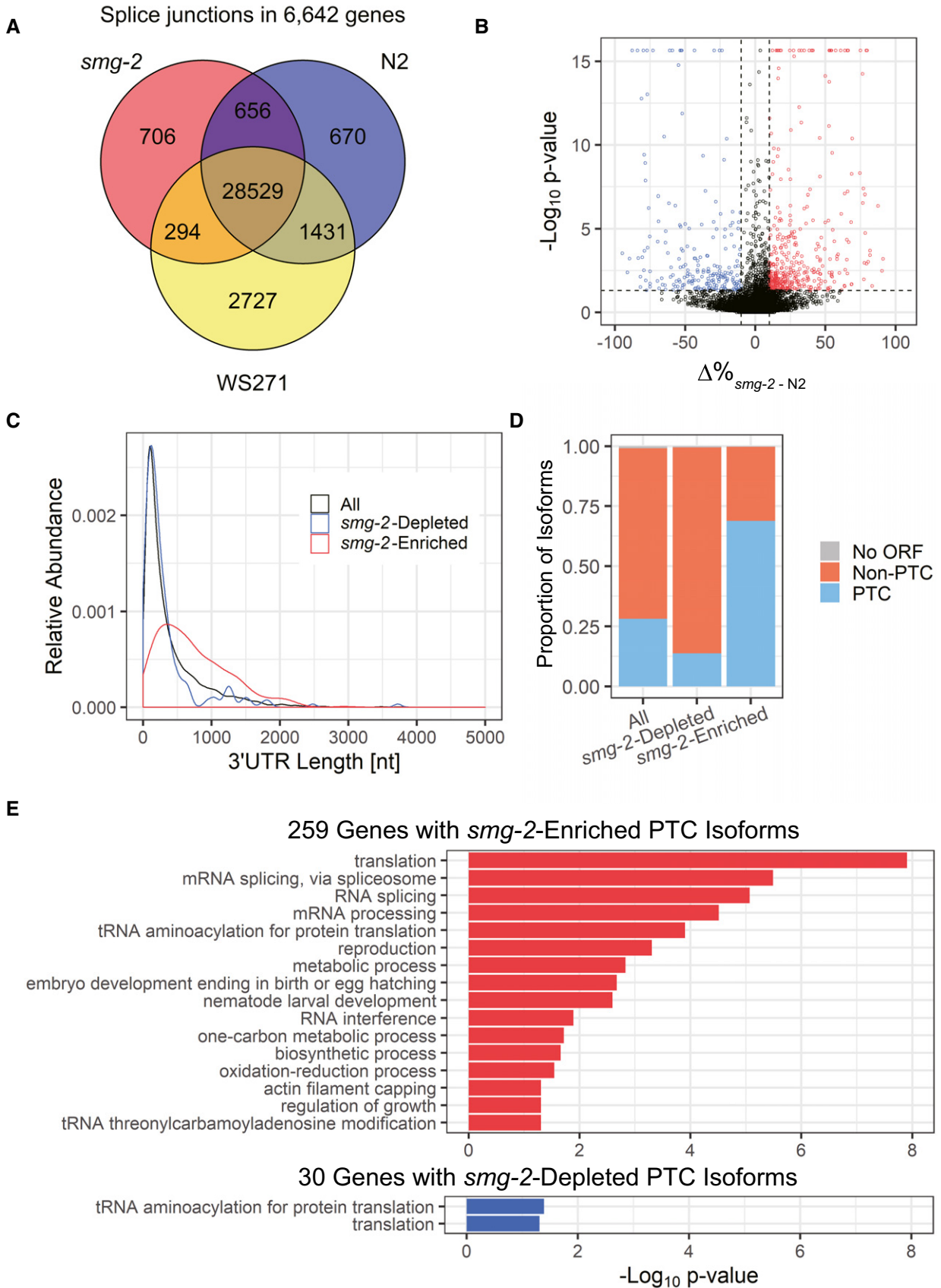
A Splice junctions in 6,642 genes

B

C

D

E

259 Genes with *smg-2*-Enriched PTC Isoforms

30 Genes with *smg-2*-Depleted PTC Isoforms

Figure 1.

isoforms within the genes remain constant throughout development and in nascent RNAs like those of ribosomal protein genes (Takei *et al*, 2016) and used the pooled data for N2. Figure 1B summarizes a difference in percentages of an mRNA isoform within the gene ($\Delta\%_{smg-2-N2}$, percentage in *smg-2* subtracted by percentage in N2) and a *P*-value for each of 8,701 isoforms. We identified 219 of *smg-2*-depleted isoforms ($\Delta\%_{smg-2-N2} < -10$, $P < 0.05$) from 208 genes and 420 of *smg-2*-enriched isoforms ($\Delta\%_{smg-2-N2} > 10$, $P < 0.05$) from 375 genes (Fig 1B and Dataset EV1). Assuming that an mRNA is translated from the first AUG codon, the *smg-2*-enriched isoforms (median = 613 nt) had significantly longer 3′ untranslated regions (3′UTRs) compared to the *smg-2*-depleted isoforms (median = 194 nt) as well as to total of 10,136 detected isoforms from 4,366 genes with at least 10 total reads in both strains (median = 218 nt) ($P < 2e-16$, Wilcoxon rank sum test) (Fig 1C). Assuming that a premature termination codon (PTC) resides > 50 nucleotides (nt) upstream from the downstream-most exon-exon junction in an mRNA, 68.8% (289/420) of the *smg-2*-enriched mRNA isoforms had PTCs, whereas only 13.7% (30/219) of the *smg-2*-depleted isoforms and 28.1% (2,851/10,136) of all detected isoforms had PTCs (Fig 1D and Dataset EV1). We performed reverse transcription (RT)-semi-quantitative polymerase chain reaction (PCR) analysis of 12 genes with *smg-2*-enriched PTC isoforms and confirmed stabilization of all the PTC isoforms in the *smg-2* mutant except for extra isoforms with retained introns (Appendix Fig S1). These results indicate that 259 genes that produces the 289 PTC-containing and *smg-2*-enriched mRNA isoforms are high-confidence genes regulated by AS-NMD in *C. elegans*.

Gene ontology (GO) analysis of the 259 genes that undergo AS-NMD revealed enrichment of genes related to RNA translation and processing (Fig 1E). This is consistent with previous findings that many of RNA-binding proteins (RBPs) including ribosomal proteins can negatively autoregulate their own expression by modulating alternative splicing patterns in both mammals and nematodes (Jangi & Sharp, 2014; Wani & Kuroyanagi, 2017).

Dynamic alternative splicing regulation of SAM synthetase genes upon feeding

Genes related to metabolism are also significantly enriched among those that undergo AS-NMD (Fig 1E). During the course of analysis of such genes, we found that alternative splicing of the *sams-3* and *sams-4* genes (Fig 2A) drastically changed upon feeding and fasting in the *smg-2* mutant (Fig 2B lanes 1–2 and Appendix Fig S2). RT-quantitative PCR (qPCR) analysis revealed 5.6-fold and 2.0-fold increase in the total amounts of *sams-3* and *sams-4* mRNAs, respectively, upon feeding and confirmed divergent changes in the

amounts the productive and PTC-containing mRNA isoforms (Fig EV1A). We confirmed that the PTC-containing *sams-3* and *sams-4* isoforms are also induced upon feeding and actually degraded by NMD in the wild-type background by feeding L1 larvae of N2 in the absence and presence of a translation inhibitor emetine that eventually inhibits the translation-dependent NMD process (Fig 2B lanes 4–6 and Fig EV1B). Alternative splicing of their paralogue *sams-5* was also dynamically regulated upon feeding and fasting (Figs 2 and EV1, Appendix Fig S2). We reasoned that expression of these genes is regulated by AS-NMD under certain environmental conditions and therefore focused on these genes in the following sections.

The *sams* genes are members of a gene family encoding SAM synthetase that produces SAM from L-methionine (L-Met) and adenosine tri-phosphate (ATP). The *C. elegans* genome contains five members of the SAM synthetase genes (Fig 2A) (Tamiya *et al*, 2013). *sams-3* and *sams-4* are highly homologous to each other (91.9% nucleotide sequence identity in the coding region), share exon organization (Fig 2A), and are divergent neighbors in the *C. elegans* genome. *sams-5* also shares the gene structure and the alternative splicing patterns (Fig 2). We noticed that nucleotide sequences of intron 2, the site of the alternative splicing regulation, in these genes are extraordinarily conserved for introns (87.5% identity between *sams-3* and *sams-4*) (Fig EV2). In contrast, *sams-1* lacks an intron at this position (Figs 2A and EV2) and is therefore constitutively expressed. *sams-2* is the most homologous to *sams-3* (94.2% overall nucleotide sequence identity), yet is a pseudogene because of a frame-shifting insertion in exon 3 (Fig EV2) and is constitutively spliced due to a substitution at the proximal 3′ splice site (SS) for intron 2 (Fig EV2).

To ask whether the feeding-induced change in the alternative splicing patterns of the *sams* genes requires newly synthesized proteins, we fed the *smg-2* worms in the presence of emetine. The ratios and the amounts of the mRNA isoforms changed to some extent even in the presence of emetine (Figs 2B and EV1). This is in good contrast to the amounts of *fat-7* and *acs-2* mRNAs whose induction and reduction, respectively, were completely suppressed by the emetine treatment (Fig EV1A). These results indicated that induction and dynamic splicing regulation of the *sams* genes do not depend on synthesis of new proteins upon feeding.

Negative feedback regulation of alternative splicing of the SAM synthetase genes

To address biological roles for the dynamic AS-NMD of the *sams* genes *in vivo*, we tested whether or not SAM synthetase activity autoregulates SAMS expression. Because *sams-1* is the only *sams*

Figure 2. Alternative splicing of *sams-3*, *sams-4*, and *sams-5* is dynamically regulated upon feeding.

A   Schematic representation of the *sams* genes in *C. elegans*. Boxes indicate exons. Coding regions of productive mRNAs are in orange. A truncated coding region with a premature termination codon in a pseudogene *sams-2* is colored cyan. Double arrows illustrate regions deleted in mutant alleles indicated.

B   Alternative splicing of *sams-3*, *sams-4*, and *sams-5* in unfed and fed worms without or with a protein synthesis inhibitor emetine. Synchronized L1 larvae of an NMD-deficient strain KH1668: *smg-2 (yb979)* (lanes 1-3) and a wild-type strain N2 (lanes 4-6) were incubated in S-complete medium alone (lanes 1, 4), with a standard *E. coli* strain OP50 (OD_{600} = 10.0) (lanes 2, 5) or OP50 supplemented with 10 mg/ml emetine (lanes 3, 6) for 3 h at 20°C. Total RNAs were extracted from whole animals and subjected to semi-quantitative RT–PCR, whose products were analyzed by capillary electrophoresis. Representative gel-like presentation is indicated (n = 3). Schematic structure of each PCR product is indicated on the right. Open reading frames (ORFs) for full-length and truncated proteins are in orange and cyan, respectively. *rpl-12* was used as an unaffected control.
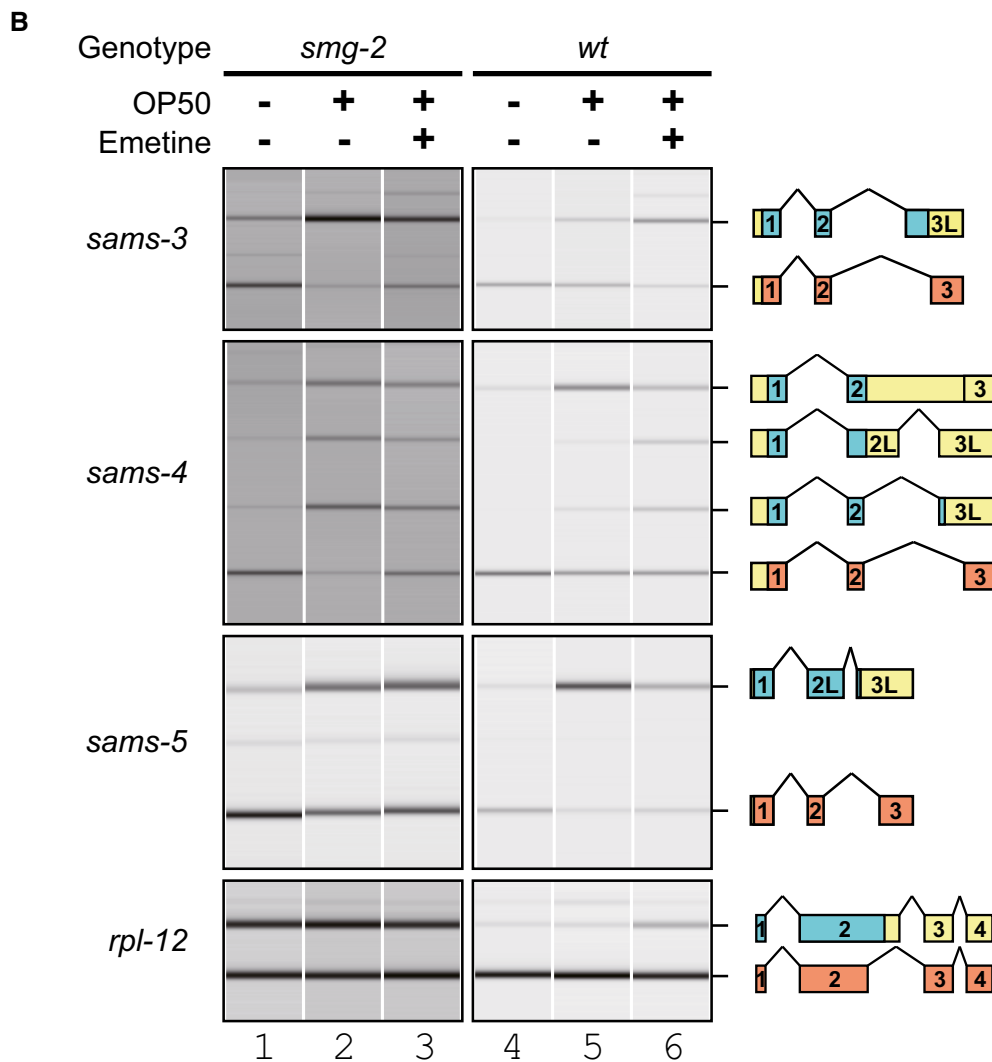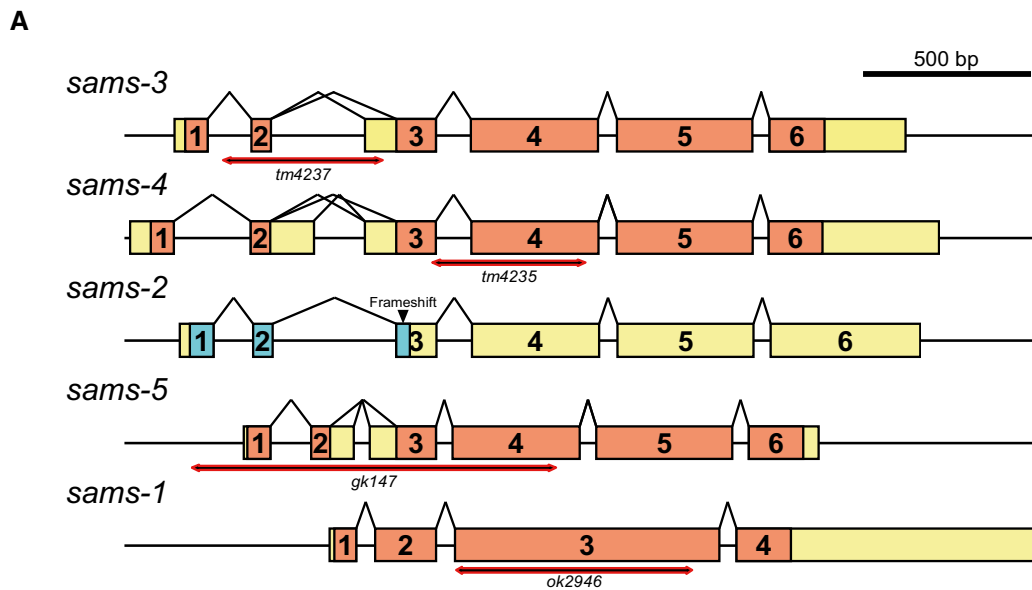
Figure 2.

gene that is constitutively expressed and because *sams-3* and *sams-4* are neighboring genes, we tested effects of deleting *sams-1* and *sams-5* on splicing patterns of *sams-3* and *sams-4* in the *smg-2* mutant background (Fig 3A). In unfed worms, the splicing patterns of *sams-3* and *sams-4* were not so much different between the *smg-2* (lane 1) and the *smg-2; sams-5; sams-1* (lane 5) mutants. Upon feeding, however, proportions of the enzyme-coding isoforms were apparently higher in the *smg-2; sams-5; sams-1* mutant (lane 6) compared to the *smg-2* mutant (lane 2). RT–qPCR analysis revealed comparable induction of total *sams-3* (5.6-fold in *smg-2* vs 6.4-fold in *smg-2; sams-5; sams-1*) and *sams-4* (1.7-fold vs 1.6-fold) mRNAs (Fig EV3A–C), indicating that disruption of *sams-1* and *sams-5* did not affect transcriptional regulation of *sams-3* or *sams-4*. Isoform-specific qPCR analysis confirmed divergence of the feeding-induced splicing change between the two strains (Fig EV3A and B). We also fed these worms in the presence of a substrate or a competitive inhibitor of SAM synthetase. The substrate L-Met had little effect (lanes 3 and 7) while the inhibitor cycloleucine (Lombardini & Talalay, 1970) slightly but significantly increased the proportions (lanes 4 and 8) and the amounts (Fig EV3A) of the productive isoform of *sams-3* in either strains. These results indicated that SAM synthase activity regulates AS-NMD of the *sams-3* and *sams-4* genes.

To test whether increase in the amounts of the productive mRNA isoforms leads to increase in the amounts of SAMS proteins, we performed Western blot analysis with antibodies specific to each of the four SAMS proteins. The amounts of SAMS-3 and SAMS-4 remain constant throughout larval development in the *smg-2* mutant, whereas they gradually increased in the *smg-2; sams-5; sams-1* mutant (Fig 3B). Consistent upregulation of SAMS-3 and SAMS-4 mRNAs and proteins in the *sams-1* mutant was observed in the wild-type background (Figs 3C and EV3D). These results indicated that homeostasis of SAM synthetase activity in *C. elegans* is maintained by negative feedback through AS-NMD of the *sams* genes.

mett-10 regulates alternative splicing of the *sams* genes *in vivo*

Because SAM is the major donor of a methyl group for methyltransferases that methylate proteins, DNAs, RNAs, or lipids (Fontecave *et al*, 2004), we speculated that altered SAM synthetase activity affects alternative splicing of the *sams* genes through altered methylation levels of specific target molecule(s) for certain methyltransferase(s). We first analyzed histone methylation levels because some of histone marks are known to affect alternative splicing by recruiting splicing factors or by affecting the transcription elongation rate in mammals (Allo *et al*, 2009; Schor *et al*, 2009; Luco *et al*, 2010; Saint-Andre *et al*, 2011). Chromatin immunoprecipitation coupled with high-throughput sequencing (ChIP-seq) analyses of

histone H3 with dimethylation on lysine 4 (H3K4me2), trimethylation on lysine 27 (H3K27me3) or trimethylation on lysine 36 (H3K36me3), however, did not reveal a significant difference at the alternatively spliced exon in the *sams-3* or *sams-4* locus between the *smg-2* and *smg-2; sams-5; sams-1* mutants (Appendix Fig S3), precluding the scenario.

We next speculated methylation of the *sams* pre-mRNAs themselves. Although the most abundant internal chemical modification in higher eukaryotic mRNAs is m^{6}A (Wei *et al*, 1975), the *C. elegans* genome lacks orthologous genes for METTL3, METTL14, and other components of mammalian m^{6}A methyltransferase complex that are responsible for the vast majority of the m^{6}A modifications (Cunningham *et al*, 2019; Arribere *et al*, 2020). Recently, it has been shown that another human methyltransferase METTL16 specifically catalyzes m^{6}A modification in a consensus sequence UACAGARAA within a loop of six hairpin structures on 3′UTR of human *MAT2A* mRNA that is translated into SAM synthetase (Pendleton *et al*, 2017; Shima *et al*, 2017; Doxtader *et al*, 2018). We noticed that each of *sams-3*, *sams-4*, and *sams-5* pre-mRNAs potentially forms a hairpin structure with a loop sequence similar to the METTL16 consensus and that the potential m^{6}A site is exactly at the invariant AG dinucleotide of the distal 3′SS that is specifically used for the productive mRNA isoform (Figs 4A and B and EV2). We therefore tested whether the METTL16 orthologue of *C. elegans*, METT-10 (Appendix Fig S4), is involved in the splicing regulation of *sams-3*, *sams-4,* and *sams-5 in vivo* (Fig 4C). The proportions of the NMD isoforms upon feeding drastically decreased in a *smg-2; mett-10* double mutant (lane 4) compared to those in the *smg-2* single mutant (lane 2), indicating that *mett-10* is required for shifting the splice site choice from the distal/productive to the proximal/unproductive 3′SSs upon feeding. We also found that the productive isoforms of *sams-3* and *sams-4* mRNAs are upregulated in a *mett-10* single mutant (Fig EV4A) and SAMS-3 and SAMS-4 protein levels are higher in the *mett-10* mutant (Fig EV4B) compared to the wild-type strain, confirming that *mett-10* is required for negative regulation of *sams-3* and *sams-4* in the wild-type background.

METT-10 specifically catalyzes the m^{6}A modification at the distal 3′SS *in vitro*

We next asked whether *C. elegans* METT-10 can directly methylate the *sams* pre-mRNAs *in vitro*. We prepared a 127-nucleotide (nt) RNA spanning from intron 2 to exon 3 of the *sams-3*/*sams-4* genes (Fig EV2) and performed *in vitro* methylation reactions with recombinant full-length METT-10 protein as well as methyltransferase domain of human METTL16. As expected, liquid chromatography (LC) coupled with tandem mass spectrometry (MS/MS) revealed that

---

Figure 3. Expression of *sams-3*, *sams-4*, and *sams-5* is negatively regulated by SAM synthetase activity through alternative splicing.

A   Alternative splicing of *sams-3*, *sams-4*, and *sams-5* in *smg-2 (yb979)* and *smg-2 (yb979); sams-5 (gk147); sams-1 (ok2946)* mutants. Synchronized L1 larvae of each strain were incubated in S-complete medium alone (lanes 1 and 5), with OP50 (OD$_{600}$ = 10.0) (lanes 2 and 6) and with OP50 supplemented with 25 mM L-Met (lanes 3 and 7) or 25 mM cycloleucine (cLeu) (lanes 4 and 8) for 3 h at 20°C. The splicing patterns were analyzed and presented as in Fig 2B (*n* = 3).

B, C   Western blot analysis of SAMS-1, SAMS-3, and SAMS-4 during larval development in the *smg-2 (yb979)* (B) and wild-type (C) backgrounds. Genotypes of the worms are *smg-2 (w)* and *smg-2; sams-5; sams-1 (s)* in (B) and wild-type *(w)* and *sams-1 (s)* in (C). Synchronized L1 larvae of each strain were incubated with OP50 at 20°C and subjected to Western blot analysis at indicated time points. Anti-β-tubulin (B) or Coomassie Brilliant Blue (CBB) staining (C) was used as a loading control. Specificity of the antibodies is confirmed in Appendix Fig S12. Note that upregulation of SAMS-1 protein in the wild type during larval development in (C) is consistent with feeding-induced upregulation of *sams-1* mRNA in Fig EV3D.
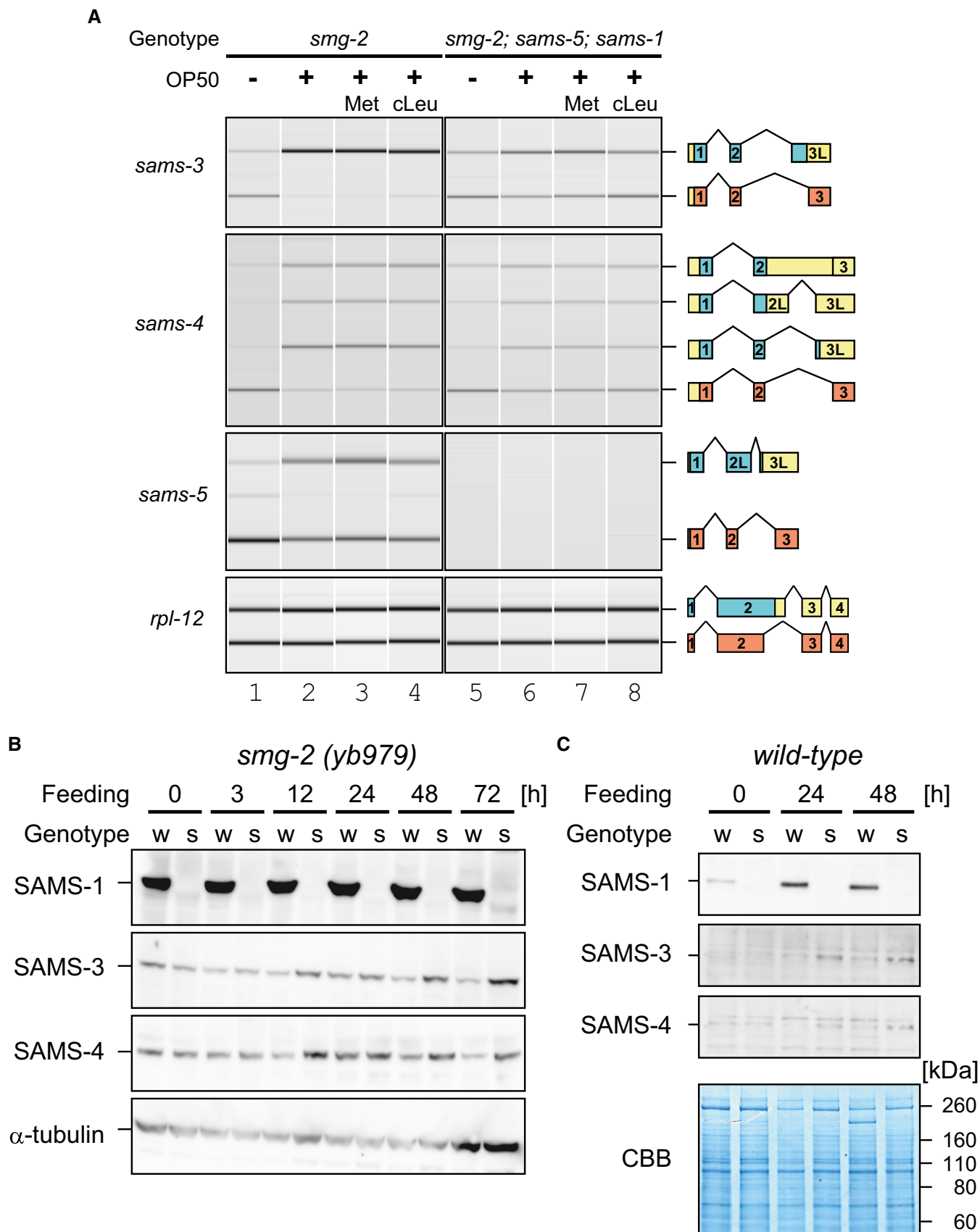
Figure 3.

these recombinant proteins specifically and efficiently methylated the adenine base within the AG dinucleotide at the distal 3′SS in a SAM-dependent manner (Fig 5A and B, Appendix Figs S5 and S6).

Endogenous *sams* mRNAs have the m⁶A modification at the distal 3′SS

We finally investigated m⁶A modification of endogenous *sams* mRNAs. The potential m⁶A modification site is at the end of intron 2 and is excised from the productive mRNA, whereas it is retained in all the NMD isoforms. RNA immunoprecipitation with an antibody specific to m⁶A (m⁶A-IP) followed by semi-quantitative RT–PCR revealed depletion of the productive mRNA and enrichment of all the NMD isoforms for *sams-3*, *sams-4*, and *sams-5* (Fig 6A). RT–qPCR analysis confirmed specific enrichment of the NMD isoforms (Fig 6B), consistent with the idea that the NMD isoforms have the m⁶A modification in the NMD-isoform-specific regions.

We further investigated m⁶A modification of the endogenous *sams* mRNAs by utilizing our direct RNA sequencing data. For comparison, we prepared barcoded, unmodified and m⁶A-modified 161-nt *sams-3*/*sams-4* and 163-nt *sams-5* pre-mRNAs *in vitro* (see Methods for details; sequences are available in Fig EV2). Specific and efficient (> 97.5%) m⁶A modification at the AG dinucleotide of the distal 3′SS of the *sams-3*/*sams-4* and *sams-5* RNAs methylated with the METTL16 methyltransferase domain was confirmed by LC-MS/MS (Appendix Fig S7). These four RNAs were pooled and subjected to Nanopore direct RNA sequencing, which records ion current signals as an RNA strand passes through a nanopore (Garalde *et al*, 2018). The *sams-3*/*sams-4* and *sams-5* RNAs were successfully distinguished by standard base-calling and mapping. There was not a crucial difference, however, between unmodified and m⁶A-modified RNAs in mean and standard deviation of the fluctuating current and duration time at each nucleotide position (Fig 6C and D, Appendix Fig S8); the unmodified and m⁶A-modified *sams-3*/*sams-4* RNAs were classified with only 64.58% of accuracy based only on the mean of the current at the m⁶A site (Fig 6D). We therefore conducted machine learning with a variety of algorithms to classify modification status of each of the *sams* RNA reads. Most of the thirteen algorithms tested successfully classified methylated test reads as "m⁶A-modified" with 86–90% sensitivity and unmethylated test reads as "unmodified" with 11–19% false positives (Figs 6E and EV5A). As expected, the means of the current and the standard deviations at and near the m⁶A modification site contributed to the successful classification as demonstrated by some of the algorithms (Figs 6F and EV5B–E). With these classifiers, 73–100% of the endogenous *sams-3* or *sams-4* mRNA isoforms carrying the

putative m⁶A modification site were classified as "m⁶A-modified" (Figs 6E and EV5A). These results indicated that most, if not all, of the NMD isoforms of the endogenous *sams* mRNAs have the m⁶A modification at the distal/productive 3′SS.

Discussion

In the present study, we demonstrated that homeostasis of SAM synthetase in *C. elegans* is regulated at the pre-mRNA splicing level of the *sams-3*, *sams-4*, and *sams-5* genes through m⁶A modification at the invariant AG dinucleotide of the distal 3′SS of intron 2 (Fig 7A). At low levels of SAM, the distal 3′SS remains unmodified and is preferentially used as a splice acceptor for the productive mRNA, which is translated into active SAM synthetase proteins that eventually increase the SAM level. At excess concentrations of SAM, the methyltransferase METT-10 specifically catalyzes the m⁶A modification at the distal 3′SS, which leads to selection of the proximal 3′SS and production of the NMD isoforms.

This is the first demonstration that the m⁶A modification at the 3′SS interferes with splicing in any organisms. The invariant AG dinucleotide at the 3′SS is recognized by a small subunit of an evolutionarily conserved heterodimeric protein complex U2 auxiliary factor (U2AF) (Merendino *et al*, 1999; Wu *et al*, 1999). In *C. elegans*, the consensus 3′SS sequence UUUUCAG is recognized by U2AF composed of the large subunit UAF-1 and the small subunit UAF-2 (Zorio & Blumenthal, 1999; Hollins *et al*, 2005). Crystal structure of the small subunit of U2AF binding to a 3′SS sequence has been solved only for the orthologue in fission yeast *Schizosaccharomyces pombe*, U2AF23, in complex with a part the large subunit U2AF59 (Yoshida *et al*, 2015; Yoshida *et al*, 2020). It has also been demonstrated that m⁶A modification of a 3′SS sequence 5′-UUAGGU-3′ at the position −2 (UUm⁶AGGU) dramatically decreased affinity to the U2AF23 complex *in vitro* (Yoshida *et al*, 2020). To ask whether m⁶A modification at the AG dinucleotide would also affect 3′SS recognition by *C. elegans* UAF-2, we modeled three-dimensional structure of UAF-2 binding to 5′-UAGGU-3′ after its homology to *S. pombe* U2AF23 (Appendix Fig S9). The amino group of the adenine base at position −2 that is methylated upon m⁶A modification is embedded in a pocket on the surface of Zn finger domain 1 (Fig 7B) and is intimately surrounded by the identical residues as *S. pombe* U2AF23 forming the pocket (Yoshida *et al*, 2020), consistent with our finding that the m⁶A modification at the invariant AG dinucleotide interferes with its use as the 3′SS (Fig 7A) even in the absence of a reader protein in *C. elegans*. As for the function of the m⁶A modification in alternative splicing regulation

---

Figure 4. *mett-10* is required for effective production of NMD isoforms from the *sams* genes *in vivo*.

A Nucleotide sequence alignment of putative stem-loop structures in the *C. elegans sams-3*, *sams-4*, and *sams-5* genes together with six hairpin structures in 3′UTR of the human *MAT2A* gene. Conserved residues are shaded in black. Loop, transition, and stem regions of the *MAT2A* hairpins (Doxtader *et al*, 2018) are boxed in magenta, green, and gray, respectively. An arrowhead indicates adenine bases in the *MAT2A* hairpins that are specifically modified into m⁶A by METTL16 *in vitro* (Shima *et al*, 2017).

B Schematic representation of the predicted hairpin structures in *sams-3*/*sams-4* (left) and *sams-5* (right) pre-mRNAs. The boundaries between intron 2 and exon 3 are indicated. Arrowheads indicate the m⁶A modification sites.

C Alternative splicing of *sams-3*, *sams-4*, and *sams-5* in *smg-2* (yb979) and *smg-2* (yb979); *mett-10* (ok2204) mutants. Synchronized L1 larvae of each strain were incubated in S-complete medium alone (lanes 1 and 3) or with OP50 (lanes 2 and 4) for 3 h at 20°C, and the splicing patterns were analyzed and presented as in Fig 2B.

Figure 4.

A

m⁶A
AUUACm⁶AGp
m/z 1139.654
z = - 2

A
AUUACAGp
m/z 1132.646
z = - 2

B
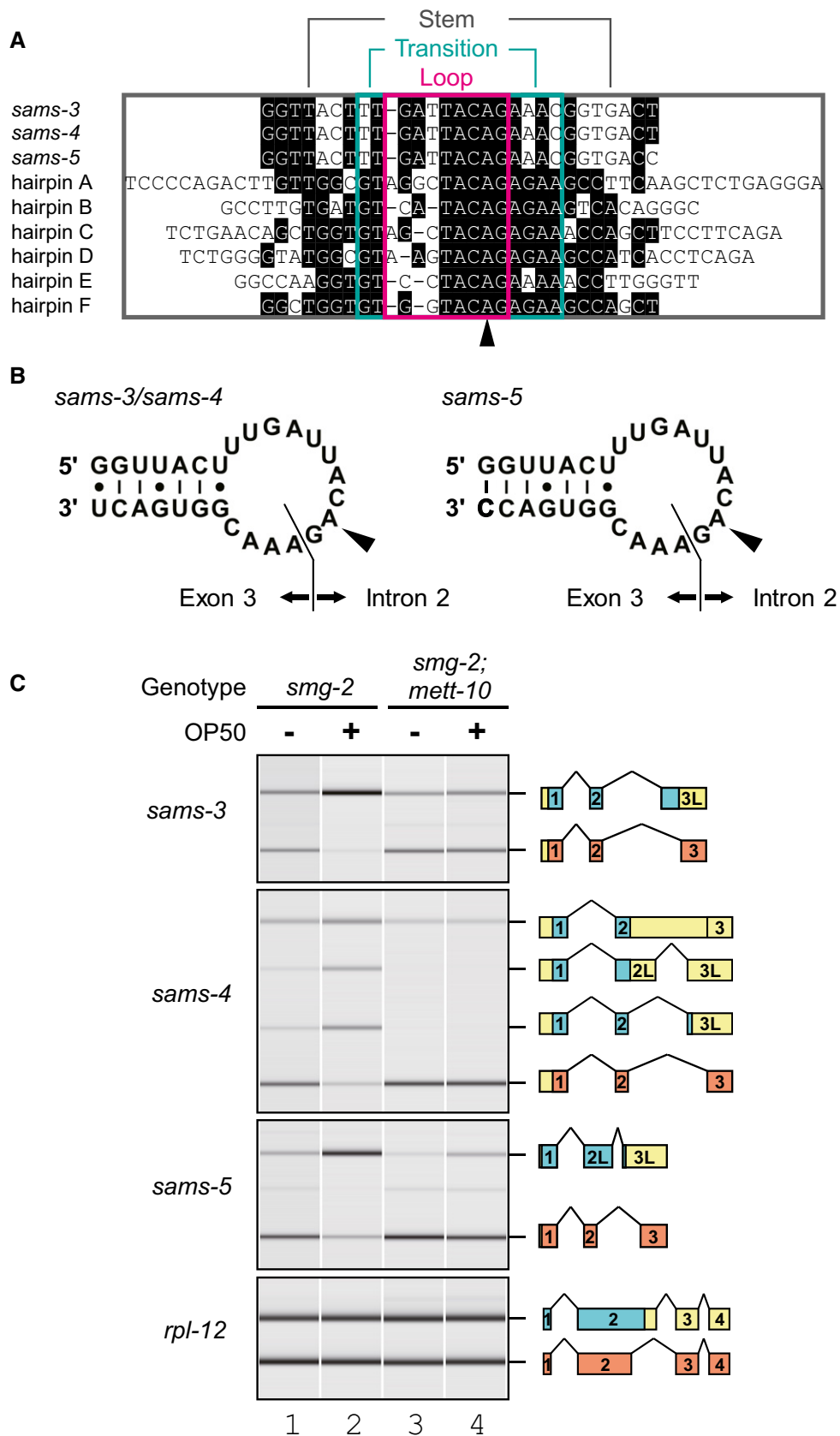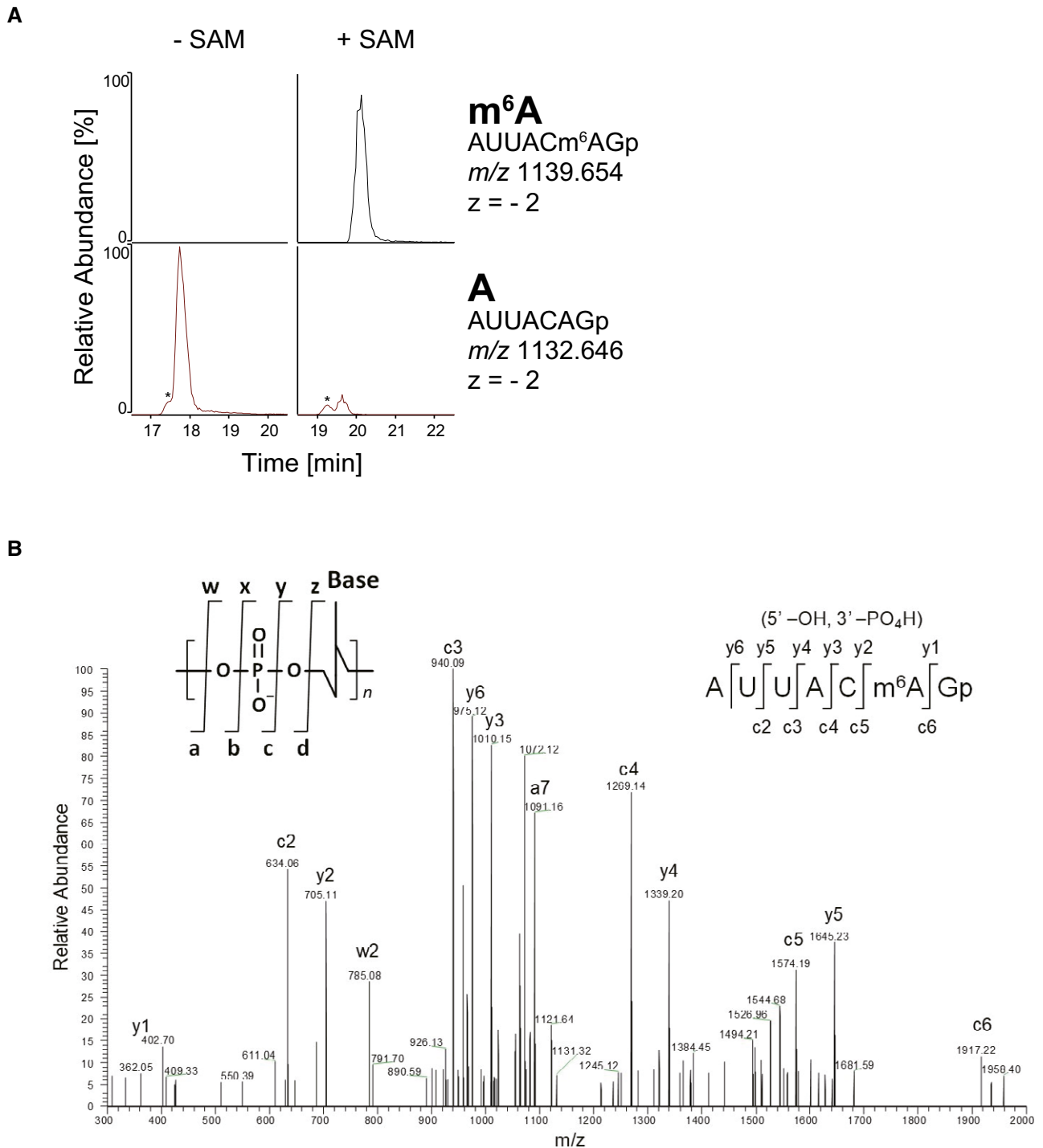
Figure 5. **METT-10 catalyzes m⁶A modification at the invariant AG dinucleotide of the distal 3′SS *in vitro*.**

A   Mass chromatograms of RNA fragments to detect m⁶A (top) or unmodified A (bottom) after *in vitro* incubation of 127-nt *sams-3/sams-4* pre-mRNA (sequence available in Fig EV2) with recombinant full-length METT-10 protein in the presence (left) or absence (right) of 1 mM SAM. The sequence, *m/z* value, and charge state for each fragment are indicated on the right. Asterisks indicate non-specific signals.

B   The negatively charged ions of RNase T1 fragment is decomposed in the instrument by collision-induced dissociation (CID) using helium gas. The product ions produced by CID are assigned on the sequence illustrated on the top right inset panel. Nomenclature of the product ions are described in the literature (McLuckey *et al*, 1992). Product ions of c and y series derive from the 5′ and 3′ termini of the fragment, respectively.

Figure 6. Endogenous unproductive *sams* mRNAs have m⁶A modification at the AG dinucleotide of the distal 3'SS.

A, B   m⁶A-IP specifically enriched *sams* mRNA isoforms that retain the AG dinucleotide at the distal/productive 3'SS. (A) Representative gel-like images (*n* = 3) of semi-quantitative RT–PCR analysis of *sams-3*, *sams-4*, and *sams-5* in input and immunoprecipitated (IP) RNAs from the *smg-2 (yb979)* mutant. The splicing patterns were analyzed and presented as in Fig 2B. (B) Relative enrichment of total and each of mRNA isoforms compared to *eef-1A*.1 mRNA by RT–qPCR. Error bars indicate standard error of mean (*n* = 3).

C   Examples of normalized Nanopore currents for unmodified and m⁶A-modified *in-vitro* transcribed *sams-3/sams-4* RNAs at nucleotide positions −4 through +4 relevant to the m⁶A site. One hundred reads are plotted for each. Color codes are indicated.

D   Distribution of mean (top) and standard deviation (bottom) of normalized Nanopore currents at nucleotide positions −4 through +4 relevant to the m⁶A site for 5,000 of the unmodified and 2,680 of the m⁶A-modified *sams-3/sams-4* RNAs and 85 of an endogenous *sams-3* mRNA isoform E2/E3L. Color codes are indicated. Central bands represent the median, boxes represent the 25th and 75th percentiles, and whiskers represent the lowest and highest values. A red line at position 0 in the top panel indicates a cutoff line (mean current = 1.7557) that discriminates between the unmodified and m⁶A-modified *sams-3/sams-4* RNAs with accuracies of 64.58% for both.

E   Machine learning-based classification of *sams* RNA reads in Nanopore direct RNA sequencing data. The statistics in (D) as well as duration time of the Nanopore current at nucleotide positions −50 through +50 of up to 80% of mapped reads from the unmodified and methylated *in vitro* transcribed *sams-3/sams-4* and *sams-5* RNAs were pooled and used for training with a machine learning algorithm Gradient Boosting and accuracy of the classifier was tested with 20% of the mapped reads. The classifier was also applied to reads identified as unproductive *sams-3*, *sams-4*, or *sams-5* mRNA isoforms in the analysis of endogenous mRNAs shown in Fig 1. Numbers of reads used in the tests are indicated at the top; percentages of reads classified as "m⁶A-modified" are shown with color code.

F   Relative importance of the statistics at each position for Gradient Boosting.

of mammalian pre-mRNAs, conflicting results have been reported (Xiao *et al*, 2016; Ke *et al*, 2017b; Louloupi *et al*, 2018; Zhou *et al*, 2019), yet there is not a reported case where the invariant AG dinucleotide at the 3'SS has the m⁶A modification.

This study demonstrated that homeostasis of SAM in *C. elegans* is maintained by an indirect negative feedback loop relying on METT-10 that utilizes SAM to catalyze m⁶A modification for AS-NMD of SAM synthetase pre-mRNAs (Fig 7A). In human cells, the mRNA level of the SAM synthetase gene *MAT2A* is also indirectly regulated by the SAM level and dual roles have been reported for METTL16 that methylates *MAT2A* mRNA on six hairpin structures in the 3'UTR; prolonged occupancy of METTL16 on the upstream-most hairpin due to lack of SAM promotes splicing of a retained

intron to maturate the *MAT2A* mRNA (Pendleton *et al*, 2017), whereas m⁶A modification of the six hairpins by METTL16 leads to nuclear degradation of the mRNA via a nuclear reader protein YTHDC1 (Bresson *et al*, 2015; Shima *et al*, 2017). SAM is the major methyl-donor reagent in all living organisms and is also used as a source of methylene groups, amino groups, ribosyl groups, and aminopropyl groups (Fontecave *et al*, 2004). Altered SAM levels affect a variety of biological processes including longevity (Hansen *et al*, 2005), lipid homeostasis (Li *et al*, 2011; Walker *et al*, 2011), and immune response (Ding *et al*, 2015) in *C. elegans* as well as longevity in *Drosophila* (Obata & Miura, 2015), maintenance and differentiation of human-induced pluripotent stem cells (iPSCs) (Shiraki *et al*, 2014), and osteoclast differentiation in the mouse
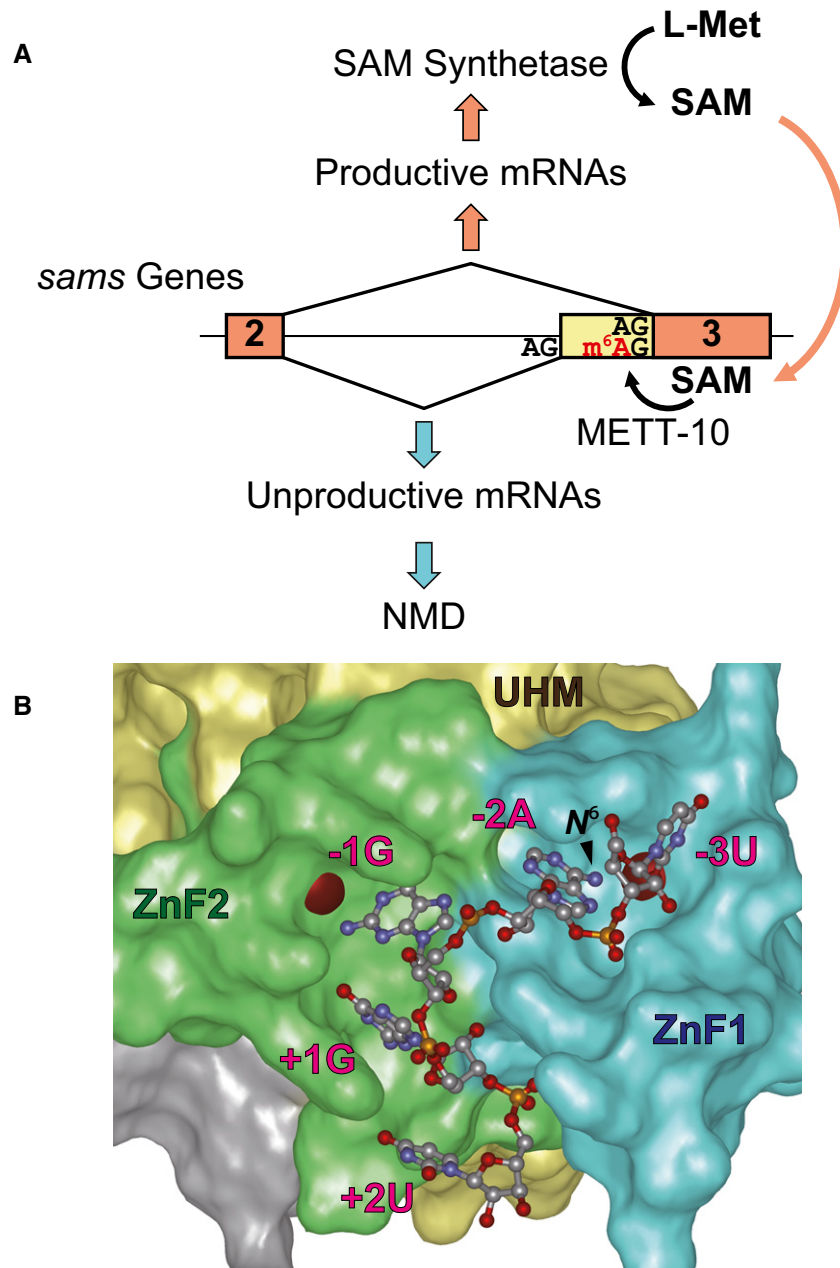
Figure 7. A model for negative feedback regulation for homeostasis of SAM synthetase genes in *C. elegans*.

A A model for AS-NMD regulation of the *sams* genes in *C. elegans*. See text for details.

B Modeled structure of *C. elegans* UAF-2 binding to 5′-UAGGU-3′. The structure was modeled based on sequence homology to U2AF23 from *S. pombe* (Appendix Fig S9) and crystal structure of *S. pombe* U2AF23/U2AF59 complex bound to the RNA (Yoshida *et al*, 2020). N-terminal Zn finger 1 (ZnF1), U2AF homology motif (UHM), and C-terminal Zn finger 2 (ZnF2) domains are colored in blue, yellow and green, respectively. Red spheres indicate zinc ions. The position of the amino group methylated upon m6A modification (N^6) is indicated with an arrowhead.

(Nishikawa *et al*, 2015). Autoregulation of SAM synthetase gene expression by alternative pre-mRNA splicing in *C. elegans* demonstrated in this study emphasizes the importance of maintaining the SAM level in eukaryotes.

We demonstrated that METT-10 as well as human METTL16 methyltransferase domain specifically methylated the adenine base

at the AG dinucleotide of the distal 3′SS of *sams-3*/*sams-4* and *sams-5* pre-mRNAs *in vitro*. A recent study on crystal structures of the METTL16 catalytic domain bound to the hairpins of the *MAT2A* mRNA revealed structural basis for recognition of the target RNAs (Doxtader *et al*, 2018). Most of the amino acid residues directly involved in recognition of the RNAs are conserved in METT-10

(Appendix Fig S4A). Each nucleotide in a UACAG stretch in the loop is directly recognized by METTL16 (Doxtader *et al*, 2018) and is perfectly conserved in the *sams* genes (Fig 4A). There is not a direct contact between METTL16 and the stem structures (Doxtader *et al*, 2018), consistent with less conserved sequences in the stem region (Fig 4A). The transition region between the loop and the stem is highly conserved among the human *MAT2A* hairpins (Fig 4A) and forms three unusual base pairs between GU and AGAA motifs (Doxtader *et al*, 2018). However, the sequence of the transition region is not well conserved in the *sams* genes (Fig 4A) and a key residue Arg200 that recognizes the transition region is not conserved in METT-10 (Appendix Fig S4A). Nevertheless, METTL16 as well as METT-10 can specifically target the AG dinucleotide of the *sams* pre-mRNAs (Fig 5 and Appendix Figs S5–S7). This is consistent with an idea that the transition region of the stem-loop is a key region to tune the methylation efficiency and not the target recognition based on previous findings that a G-to-A substitution in the latter motif or an R200Q substitution rather increased the *in vitro* methylation activity of METTL16 (Doxtader *et al*, 2018). Considering that regulation of *sams* gene expression is based on balanced competition between splicing and m^{6}A modification (Fig 7A), it is reasonable to suggest that highly conserved nucleotide sequences flanking the distal as well as proximal 3′SSs of intron 2 (Appendix Fig S10) play critical roles in the genus *Caenorhabditis*. *MAT2A* and *sams* mRNAs are so far the only known mRNA targets for human METTL16 and *C. elegans* METT-10, respectively. Although the m^{6}A modification is very rare (0.0008%) in *C. elegans* mRNAs (Liberman *et al*, 2020), this study revealed the critical and specific role for the m^{6}A modification in the mRNA metabolism. Quite recently, Mendel *et al* (2021) have reached essentially the same conclusion with distinct approaches.

We performed long-read direct RNA sequencing of poly(A)$^+$ RNAs from L1 larvae of the *smg-2* mutant of *C. elegans* and revealed full-length sequences of 3,056 splice variants that are not registered as gene models in WormBase including 1,532 variants with novel junctions and 1,963 putative NMD isoforms with PTCs. This result indicates that the long-read sequencing is a powerful tool to elucidate the full-length sequences of mRNAs and hence the repertoire of the isoforms.

We demonstrated that a metabolite SAM can negatively regulate expression of the SAM-synthesizing enzyme genes through AS-NMD for homeostasis. It is common in bacteria that metabolites directly and specifically bind to mRNAs to regulate their transcription and/ or translation for feedback regulation (Pavlova *et al*, 2019), including SAM (McDaniel *et al*, 2003; Winkler *et al*, 2003; Montange & Batey, 2006). This study identified many non-RBP genes whose expression may be regulated through AS-NMD in *C. elegans* (Fig 1E). *mett-10* is among the genes whose novel isoforms were discovered in this study and have a putative PTC. We found that the PTC-containing isoform of *mett-10* is stabilized in the *smg-2* mutant (Appendix Fig S4B and C), confirming that *mett-10* is also regulated by AS-NMD. Further studies on splicing regulation of such genes will elucidate further examples of gene expression control by environmental conditions at the pre-mRNA splicing level.

We conducted machine learning to classify m^{6}A modification status at a single specific position in individual reads for the *sams* mRNA isoforms from the direct Nanopore RNA sequencing data (Fig 6D) because the properties of the electric current were not so much different between unmodified and m^{6}A-modified RNAs prepared *in vitro* (Fig 6C). Sequencing with the Nanopore technology deconvolutes changes in the electric current as a single stranded RNA transverses a pore protein (Garalde *et al*, 2018). Since the measured current fluctuated even while the RNA strand stays in a given position, we considered not only the mean but also the standard deviation of the recorded electric current as well as the duration time at each position in the machine learning. Unbiased parameter tuning for higher accuracy revealed major contribution of the mean and the standard deviation of the electric current at the relevant positions (Figs 6E and EV5B–E), indicating that these features are useful for classifying the base modifications. The direct Nanopore RNA sequencing technology has recently been applied by other groups to detecting the m^{6}A modifications. Liu *et al* (2019) reported that systematic errors and decreased base-calling qualities can predict m^{6}A RNA modifications. Parker *et al* (2020) also reported higher base-calling error rates for an m^{6}A-modified RNA than an unmodified RNA and identified > 17,000 possible m^{6}A modification sites with a motif DRAYH in mRNAs from a plant *Arabidopsis thaliana* by comparing the error rates for an m^{6}A-writer mutant line to those for a complemented line. The differential error rate and base quality, however, were not evident in our direct RNA sequencing data for *in vitro*-modified *sams-3*/*sams-4* or *sams-5* RNAs (Appendix Fig S11), suggesting that the differential error rate analysis approach may be context-dependent. Lorenz et al developed a software MINES to detect m^{6}A modifications in mammalian mRNAs *de novo* (Lorenz *et al*, 2020), yet it relies on rich data of verified m^{6}A modification sites from cross-linking and immunoprecipitation with high-throughput sequencing (CLIP-seq) and a well-established motif DRACH for the METTL3/METTL14 complex (Linder *et al*, 2015; Ke *et al*, 2017b). Thus, classification of the base modification status at a given or new site in individual direct sequencing reads is still challenging and requires a high-quality training data set or a large number of reads with a writer mutant control.

Materials and Methods

Worm strains

Genotypes of the strains used are summarized in Appendix Table S1. Some of the strains were obtained from *Caenorhabditis* Genetics Center (CGC) and National BioResource Project (NBRP), Japan. All worms were cultured at 20°C unless otherwise mentioned. KH2418: *smg-2 (yb979); sams-1 (ok2946)*, KH2421: *smg-2 (yb979); sams-5 (gk147); sams-1 (ok2946);* and VC2428: *sams-1 (ok2946) X* were maintained in the presence of 20 mM choline chloride (Nacalai Tesque) (Walker *et al*, 2011).

Synchronized worm preparation

Gravid worms raised in S-complete medium (Lewis & Fleming, 1995) supplemented with an *E. coli* strain OP50 were bleached with standard bleaching solution (Lewis & Fleming, 1995). Embryos were harvested and washed three times with M9 buffer. The embryos were incubated in M9 buffer for 18 h (except for the *smg-2; mett-10* mutant that was incubated for 24 h) with gentle agitation for hatching and the L1 larvae were harvested and washed with S-complete.

Direct RNA sequencing

Synchronized L1 larvae of KH1668: *smg-2 (yb979)* were fed with OP50 in S-complete medium supplemented with 4 mM 4-thiouracil (4TU) (Tokyo Chemical Industry) for 6 h with gentle agitation. The worms were harvested and washed with M9, and total RNAs were extracted from the whole animals by using RNeasy Plus Mini (QIAGEN) as described previously (Kuroyanagi *et al*, 2010; Kuroyanagi *et al*, 2013). Thio-labeled RNAs were purified essentially as described previously (Duffy *et al*, 2015) with minor modification; 4TU-labeled RNAs were biotinylated with MTSEA biotin-XX (Biotium) in 90% dimethylformamide at 10°C for 30 min and purified by using Streptavidin Mag Sepharose (GE Healthcare). Ribosomal RNAs were then removed with Ribo-Zero Gold rRNA Removal Kit (Epidemiology) (Illumina), and the remaining RNAs were subjected to direct RNA sequencing. Nanopore libraries were prepared from 500 ng RNAs and sequenced using SQK-RNA002 kit and FLO_MIN107 flow cells on MinION of Oxford Nanopore Technologies (ONT) according to manual instructions. Nanopore reads of Poly(A)$^+$ RNA from the *smg-2 (yb979)* mutant and *in vitro* transcribed *sams* RNAs were base-called using Guppy version 2.3.4 and 3.0.3 (ONT), respectively, with default RNA parameters. Demultiplexing reads of the *in vitro* methylated RNAs and unmodified RNAs was performed by using fast5_subset (ONT) and in-house R scripts by checking 5′-GUCAUCCC-3′ (unmodified) and 5′-GUCAUGGG-3′ (m^{6}A) sequences within 40 nt region from the 3′-end of the reads with 1 nt mismatch/indel allowance.

Transcript annotations from Nanopore data

Nanopore direct RNA sequencing reads for the *smg-2 (yb979)* mutant and those for N2 (Roach *et al*, 2020) were mapped to ce11 reference genome in WormBase (https://parasite.wormbase.org) by using minimap2 version 2.17 (Li, 2018) with "-x splice". For the N2 data, reads of all developmental stages were pooled before mapping. Full-length transcript annotations were generated from minimap2 bam outputs using spliced_bam2gff and cluster_gff in Pinfish version 0.1.0 (ONT) with settings "-c 3 -d 2 -e 30". The transcripts were collapsed using collapse_partials in Pinfish with "-d 2 -e 30 -f 1000". The generated annotations were labeled with gene names in WormBase (WS271) using bedtools intersectBed version 2.27.1 (Quinlan & Hall, 2010). To filter truncated transcripts, annotations with 5′-ends not within +/−100 nt of annotated 5′-ends in WormBase (WS271) were discarded. Furthermore, artificial transcripts with splice junctions caused by base-calling error were filtered using supporting junction reads of Illumina RNA-seq data and annotated junctions in WormBase (WS271). The supporting junctions were generated from published Illumina RNA-seq data of N2 and the *smg-2* mutants with DDBJ accession numbers DRX002713 (Kuroyanagi *et al*, 2013), DRX021821 and DRX021822 (Takei *et al*, 2016), SRX2516749, SRX2516750, SRX2516753, and SRX2516754 (Son *et al*, 2017). The Illumina reads were mapped to ce11 reference genome using STAR version 2.5.3a (Dobin *et al*, 2013) with options "--alignIntronMin 20 --alignIntronMax 10000 --alignMatesGapMax 10000". The STAR mapping outputs include a list of splice junctions. Transcripts containing not-supported, not-annotated junctions were discarded by in-house R and Python scripts.

Analysis of putative NMD isoforms using Nanopore data

Differential isoform analysis was performed on isoforms generated from pooled Nanopore data for N2 (Roach *et al*, 2020) and the *smg-2 (yb979)* mutant by using Pinfish in the same way as described above. The read number of each isoform was extracted by using Pinfish and compared between N2 and the *smg-2* mutant by Fisher's exact tests with BH adjustment (Benjamini & Hochberg, 1995) to calculate FDR. Open reading frames (ORFs) in the isoforms were predicted by using predORF in systemPipeR version 3.10 (Backman & Girke, 2016) and the upstream-most ORFs were used. ORFs in isoforms deposited in WormBase (WS271) were re-defined in the same way. A premature termination codon (PTC) was annotated when the stop codon locates > 50 nt upstream from the last exon-exon junction. Gene ontology (GO) analysis was performed on *smg-2*-enriched PTC isoforms ($\Delta\%_{smg\text{-}2\text{-}N2} > 10$, $P < 0.05$), and *smg-2*-depleted PTC isoforms ($\Delta\%_{smg\text{-}2\text{-}N2} < -10$, $P < 0.05$) by using DAVID version 6.8 (Huang *et al*, 2009) with the genome background "*Caenorhabditis elegans*".

Total RNA extraction and RT–PCR

Synchronized L1 larvae were incubated in 400 µl of S-complete medium (Lewis & Fleming, 1995) in 1.5-ml non-stick tubes (Ambion) with continual agitation at 1,400 rpm on Thermomixer (Eppendorf). Worms were washed three times with M9 buffer, and total RNAs were extracted as described previously (Kuroyanagi *et al*, 2010; Kuroyanagi *et al*, 2013). RT–PCR was performed essentially as described previously (Kuroyanagi *et al*, 2010; Kuroyanagi *et al*, 2013). The PCR products were analyzed by using 2100 BioAnalyzer (Agilent Technologies). qPCR was performed with LightCycler 480 (Roche) and SYBR Premix DimerEraser (TaKaRa). Sequences of the primers used in the semi-quantitative RT–PCR and RT–qPCR experiments are available in Appendix Tables S2 and S3, respectively. Sequences of the PCR products were confirmed by direct sequencing or by cloning and sequencing.

Western blotting

Synchronized L1 larvae were incubated in 400 µl of S-complete medium (Lewis & Fleming, 1995) in 1.5-ml non-stick tubes (Ambion) with continual agitation at 1,400 rpm on Thermomixer (Eppendorf). Worm lysates were extracted from the synchronized worms, separated by neutral polyacrylamide gel electrophoresis (NuPAGE, Invitrogen), and transferred to nitrocellulose membrane (Protran NC, Amersham). Western blotting was performed with 1:1,000-diluted rabbit anti-SAMS antisera and 1:1,000-diluted HRP-conjugated anti-rabbit IgG antibody (Pierce). Chemiluminescence signals (West Dura, Thermo or Western BLoT Ultra Sensitive HRP Substrate, Takara) were detected by using LAS4000 (GE Healthcare). The rabbit anti-SAMS-1, anti-SAMS-3, and anti-SAMS-4 antisera were raised with synthetic peptides KALKISPALLEKAKGNPI, DVELLKKIGGKTISNGN, and SADM-LAKSQGPAQPDV, respectively, by Sigma-Aldrich Japan.

ChIP-seq analysis of histone methylations

Synchronized L1 larvae of the *smg-2* and *smg-2; sams-5; sams-1* mutants were fed with OP50 in S-complete medium for 30 min. The

worms were then washed with M9, frozen in liquid nitrogen, and ground to powder with mortar and pestle. The worm powder was treated with 1% formaldehyde at 20°C for 10 min, and cell nuclei were collected by centrifugation at 1,000 g. The chromatin was solubilized with Covaris M220 (Peak Incident Power = 75 W; Duty Factor = 20%; Cycles Per Burst = 200; time = 1,800 s). Nucleosomes with modified histones were immunoprecipitated with mouse monoclonal antibodies (MABI0303, MABI0323, or MABI0333, MBL, Nagoya, Japan) and DNAs were purified with NucleoSpin Gel and PCR Clean-up (MACHEREY-NAGEL) after proteinase K digestion of proteins at 55°C and reverse crosslinking at 65°C overnight. Sequencing libraries were prepared with TruSeq ChIP Library Prep Kit (Illumina), and sequencing (Single End 50 bp) was performed with Hiseq3000 (Illumina). Low-quality reads were trimmed by using Trimmomatic version 0.36 (Bolger *et al*, 2014) with options "-phred33 LEADING:30 TRAILING:30 MINLEN:50". Mapping to the ce11 reference genome was done by using Bowtie2 version 2.4.1 (Langmead & Salzberg, 2012) with default settings. Differentially bound regions were detected by using csaw (Lun & Smyth, 2016). In the csaw analysis, the ce11 genome was binned into 200-bp windows with a step size of 100 bp. Normalized read counts of each window were compared between the *smg-2* and *smg-2; sams-5; sams-1* mutants. Significantly changed regions were selected as those windows with $P < 0.01$. Genome browser snapshots were generated by using Integrative Genomics Viewer (Robinson *et al*, 2011).

In vitro methylation

Recombinant His-tagged full-length METT-10 and human METTL16 catalytic domain were expressed in *E. coli* and purified with HisTrap and Capto SP cation exchange columns. A template for the 127-nt *sams-3/sams-4* RNA was amplified from a synthetic oligonucleotide 5′-AACAATATGTTTCTTTACCTGTTACAACGGTTACTTTGATTACA GAAACGGTGACTAAAACGGGTATGAT-3′ with 5′-GCTAATACGACT CACTATAGGGAAACGGGGCTGAAGCTTATCGCAACAATATGTTTC TTTACCTGTTAC-3′, and 5′-CAGCTTTCGAGGTGATCTCACCGCAC AACATGATCATACCCGTTTTAGTCACC-3′. The template DNA was transcribed *in vitro* with recombinant T7 RNA polymerase. *In vitro* methylation of the *sams-3/sams-4* RNA was performed with 0.2 μM recombinant protein and 2 μM RNA in methylation buffer (20 mM HEPES-KOH pH 7.5, 150 mM NaCl, and 1 m DTT) with or without 1 mM SAM at 37°C for 3 h in a 50 μl reaction mixture.

Mass spectrometry

Identification of modified bases was performed essentially as described previously (Shima *et al*, 2017). Collision-induced dissociation (CID) spectrum analysis was performed as described previously (Shima *et al*, 2017).

Preparation of *in-vitro* methylated RNAs for direct RNA sequencing

sams-3/sams-4 and *sams-5* genomic DNA fragments were amplified from N2 genomic DNA by using PrimeStar GXL (Takara). The *sams-3/sams-4* and *sams-5* DNA fragments were further amplified with a forward primer 5′-TAATACGACTCACT ATAGGGAAACGGGGCTGA AGC-3′ (*sams-3/sams-4*) or 5′-TAATACGACTCACTATAGGGTGAC AAGA GGAT GAAAC-3′ (*sams-5*) and a barcoded reverse primer

5′-TTTTTTTTTTTTTTTTTTTTTTTGGGGGGGGGGATGACGTTTCGGACGAG AAC-3′ (C9A20) or 5′-TTTTTTTTTTTTTTTTTTTT TTTCCCCCCCCCAT GACGTTTCGGACGAGAAC-3′ (G9A20) to attach a T7 promoter and a C9A20 or G9A20 tail. The four DNA fragments were utilized as templates for *in vitro* transcription with T7 RNA polymerase, and the RNAs were purified with PAGE and gel extraction. The G9A20-tagged *sams-3/sams-4* and *sams-5* RNAs were subjected to methylation reaction with 30 μM of recombinant human METTL16 catalytic domain protein in the methylation buffer described above with 1 mM SAM at 37°C for 3 h in a 50 μl reaction mixture and were purified again with PAGE and gel extraction. The four RNA samples were then pooled and subjected to direct RNA sequencing.

m⁶A RNA immunoprecipitation

Total RNAs were extracted from synchronized L1 larvae of the *smg-2* mutant after feeding with OP50 in S-complete medium for 3 h. Immunoprecipitation of m⁶A RNA was performed by using Rabbit anti-m⁶A antibody (ab151230, Abcam) and Dynabeads Protein A (Invitrogen). Antibody-bound magnetic beads were prepared by following manual instructions and washed with Binding buffer (10 mM Tris–HCl pH 7.5, 150 mM NaCl, 0.5% NP-40) three times. Total RNAs in 30 μl of TE buffer were denatured for 5 min at 65°C, and then, the RNAs were added to the antibody-bound beads in 270 μl of Binding buffer and incubated on a mixer for 2 h at 4°C (40 μg of total RNAs and 3 μg of anti-m⁶A antibody per sample). After incubation, the beads were washed with Binding buffer twice and Wash buffer (10 mM Tris–HCl pH 7.5, 1 M NaCl, 1% NP-40) three times. Washed beads were suspended in 50 μl of RLT buffer (QIAGEN) and incubated on a mixer for 5 min at r.t. to elute the beads-bound RNAs. Finally, the eluted RNAs were purified by using RNA Clean & Concentrator-5 kit (Zymoresearch) and were subjected to semi-quantitative RT–PCR and RT–qPCR analysis.

Classification of m⁶A-modified *sams* RNAs

Raw Nanopore current data for *in vitro* prepared RNAs and the endogenous mRNAs from the *smg-2* mutant were mapped to *sams* transcript annotations generated by Pinfish using Tombo version 1.5 (ONT). Mean, standard deviation (STD), and duration time of the normalized current at each genomic position were extracted by using Tombo Python API. For machine learning, the data of the normalized current at positions from −50 through +50 relevant to the m⁶A site were used. Among 15,706 reads for the unmodified RNAs and 6,063 reads for the m⁶A-modified RNAs, up to 80% were used to train classifiers, and 20% were used for tests. The reads for the unmodified RNAs in the training data set were downsampled to the same number as those of the m⁶A-modified RNAs in order to prevent biased learning. To select the best performing models, we compared classifiers xgboost version 1.0.0 (https://github.com/dmlc/xgboost) (Chen & Guestrin, 2016) and LightGBM version 2.3.2 (https://github.com/microsoft/LightGBM) (Ke *et al*, 2017a) and those in scikit-learn version 0.22 (https://github.com/scikit-learn/scikit-learn) (Pedregosa *et al*, 2011). Scikit-learn includes a variety of algorithms including Decision Tree, Random Forest, Logistic Regression, K-Nearest Neighbor, SVM, Linear Discriminant Analysis, Quadratic Discriminant Analysis, Multilayer Perceptron, Gaussian Naive Bayes, and Adaptive Boosting. Each classifier was tuned by

grid-search of hyperparameters by using hyperopt version 0.2.2 (https://github.com/hyperopt/hyperopt) (Bergstra *et al*, 2013).

Protein sequence analysis

Multiple sequence alignment with the Clustal V or W algorithm was performed by using a module MegAlign in Lasergene 15 (DNASTAR). Modeling of the three-dimensional structure of UAF-2 was performed by using Modeller 9.24 (Webb & Sali, 2016) after the structure of *S. pombe* U2AF23 in complex with U2AF59 and 5′-UAGGU-3′ (PDB Acc. No. 7C06). The 3D structures were analyzed and visualized with a module Protean 3D in Lasergene 17 (DNASTAR).

Data availability

- RNA-Seq data: DDBJ Sequence Read Archive (DRA) DRX184564 (https://ddbj.nig.ac.jp/DRASearch/experiment?acc = DRX184564).
- RNA-Seq data: DDBJ Sequence Read Archive (DRA) DRX184565 (https://ddbj.nig.ac.jp/DRASearch/experiment?acc = DRX184565).
- Chip-Seq data: DDBJ Sequence Read Archive (DRA) DRA009050 (https://ddbj.nig.ac.jp/DRASearch/submission?acc = DRA009050).
- Codes used in the sequence analysis: GitHub KUROYANAGI-Lab/ WATABE-SAMS (https://github.com/KUROYANAGI-Lab/WATABE-SAMS).
- Nucleotide sequence: DDBJ/ENA/GenBank LC603057 (http://gete ntry.ddbj.nig.ac.jp/getentry/na/LC603057?filetype = html).
- The materials generated and/or analyzed during the current study are available from KUROYANAGI Hidehito (hidehito@med.u-ryu kyu.ac.jp).

Expanded View for this article is available online.

Author contributions

EW contributed to sequencing library preparation, bioinformatics analysis, RNA-IP, and Western blotting. MT-O and HK contributed to RT–PCR and RT– qPCR analysis. YI and TS contributed to *in vitro* methylation, and LC-MS/MS. SW, MK-A, SH, and ST contributed to preliminary data acquisition. KH and AF contributed to antibody preparation and validation. YS contributed to RNA and ChIP sequencing. HK organized the study and prepared worm strains. EW and HK wrote the manuscript.

Conflict of interest

The authors declare that they have no conflict of interest.

References

Alló M, Buggiano V, Fededa JP, Petrillo E, Schor I, de la Mata M, Agirre E, Plass M, Eyras E, Elela SA *et al* (2009) Control of alternative splicing through siRNA-mediated transcriptional gene silencing. *Nat Struct Mol Biol* 16: 717 − 724

Arribere JA, Kuroyanagi H, Hundley HA (2020) mRNA editing, processing and quality control in *Caenorhabditis elegans*. *Genetics* 215: 531 − 568

Backman TWH, Girke T (2016) systemPipeR: NGS workflow and report generation environment. *BMC Bioinformatics* 17: 388

Barberan-Soler S, Lambert NJ, Zahler AM (2009) Global analysis of alternative splicing uncovers developmental regulation of nonsense-mediated decay in *C. elegans*. *RNA* 15: 1652 − 1660

Barberan-Soler S, Zahler AM (2008) Alternative splicing regulation during *C. elegans* development: splicing factors as regulated targets. *PLoS Genet* 4: e1000001

Benjamini Y, Hochberg Y (1995) Controlling the false discovery rate: a practical and powerful approach to multiple testing. *J Roy Stat Soc: Ser B* 57: 289 − 300

Bergstra J, Yamins D, Cox DD (2013) Making a science of model search: hyperparameter optimization in hundreds of dimensions for vision architectures. *Proceedings of the 30th International Conference on International Conference on Machine Learning - Volume 28*; Atlanta, GA, USA. JMLR.org.

Bolger AM, Lohse M, Usadel B (2014) Trimmomatic: a flexible trimmer for Illumina sequence data. *Bioinformatics* 30: 2114 − 2120

Bresson SM, Hunter OV, Hunter AC, Conrad NK (2015) Canonical poly(A) polymerase activity promotes the decay of a wide variety of mammalian nuclear RNAs. *PLoS Genet* 11: e1005610

Celik A, Baker R, He F, Jacobson A (2017) High-resolution profiling of NMD targets in yeast reveals translational fidelity as a basis for substrate selection. *RNA* 23: 735 − 748

Chapin A, Hu H, Rynearson SG, Hollien J, Yandell M, Metzstein MM (2014) In vivo determination of direct targets of the nonsense-mediated decay pathway in *Drosophila*. *G3* 4: 485 − 496

Chen T, Guestrin C (2016) XGBoost: A Scalable Tree Boosting System. *Proceedings of the 22nd ACM SIGKDD International Conference on Knowledge Discovery and Data Mining*; San Francisco, California, USA. Association for Computing Machinery.

Colombo M, Karousis ED, Bourquin J, Bruggmann R, Muhlemann O (2017) Transcriptome-wide identification of NMD-targeted human mRNAs reveals extensive redundancy between SMG6- and SMG7-mediated degradation pathways. *RNA* 23: 189 − 201

Consortium CeS (1998) Genome sequence of the nematode *C. elegans*: a platform for investigating biology. *Science* 282: 2012 − 2018.

Cunningham F, Achuthan P, Akanni W, Allen J, Amode M, Armean IM, Bennett R, Bhai J, Billis K, Boddu S *et al* (2019) Ensembl 2019. *Nucleic Acids Res* 47: D745 − D751

van Delft P, Akay A, Huber SM, Bueschl C, Rudolph KLM, Di Domenico T, Schuhmacher R, Miska EA, Balasubramanian S (2017) The profile and dynamics of RNA modifications in animals. *ChemBioChem* 18: 979–984

Ding W, Smulan LJ, Hou NS, Taubert S, Watts JL, Walker AK (2015) s-Adenosylmethionine levels govern innate immunity through distinct methylation-dependent pathways. *Cell Metab* 22: 633–645

Dobin A, Davis CA, Schlesinger F, Drenkow J, Zaleski C, Jha S, Batut P, Chaisson M, Gingeras TR (2013) STAR: ultrafast universal RNA-seq aligner. *Bioinformatics* 29: 15–21

Doxtader KA, Wang P, Scarborough AM, Seo D, Conrad NK, Nam Y (2018) Structural basis for regulation of METTL16, an S-adenosylmethionine homeostasis factor. *Mol Cell* 71: 1001–1011.e4

Duan HC, Wang Y, Jia G (2019) Dynamic and reversible RNA N^6-methyladenosine methylation. *Wiley Interdiscip Rev RNA* 10: e1507

Duffy EE, Rutenberg-Schoenberg M, Stark CD, Kitchen RR, Gerstein MB, Simon MD (2015) Tracking distinct RNA populations using efficient and reversible covalent chemistry. *Mol Cell* 59: 858–866

Fontecave M, Atta M, Mulliez E (2004) S-adenosylmethionine: nothing goes to waste. *Trends Biochem Sci* 29: 243–249

Frye M, Jaffrey SR, Pan T, Rechavi G, Suzuki T (2016) RNA modifications: what have we learned and where are we headed? *Nat Rev Genet* 17: 365–372

Garalde DR, Snell EA, Jachimowicz D, Sipos B, Lloyd JH, Bruce M, Pantic N, Admassu T, James P, Warland A *et al* (2018) Highly parallel direct RNA sequencing on an array of nanopores. *Nat Methods* 15: 201–206

Hamid FM, Makeyev EV (2014) Emerging functions of alternative splicing coupled with nonsense-mediated decay. *Biochem Soc Trans* 42: 1168–1173

Hansen M, Hsu AL, Dillin A, Kenyon C (2005) New genes tied to endocrine, metabolic, and dietary regulation of lifespan from a *Caenorhabditis elegans* genomic RNAi screen. *PLoS Genet* 1: 119–128

He F, Jacobson A (1995) Identification of a novel component of the nonsense-mediated mRNA decay pathway by use of an interacting protein screen. *Genes Dev* 9: 437–454

Hollins C, Zorio DA, MacMorris M, Blumenthal T (2005) U2AF binding selects for the high conservation of the *C. elegans* 3' splice site. *RNA* 11: 248–253

Huang DW, Sherman BT, Lempicki RA (2009) Systematic and integrative analysis of large gene lists using DAVID bioinformatics resources. *Nat Protoc* 4: 44–57

Huang H, Weng H, Chen J (2020a) The biogenesis and precise control of RNA m⁶A methylation. *Trends Genet* 36: 44–52

Huang H, Weng H, Chen J (2020b) m⁶A modification in coding and non-coding RNAs: roles and therapeutic implications in cancer. *Cancer Cell* 37: 270–288

Jangi M, Boutz PL, Paul P, Sharp PA (2014) Rbfox2 controls autoregulation in RNA-binding protein networks. *Genes Dev* 28: 637–651

Jangi M, Sharp PA (2014) Building robust transcriptomes with master splicing factors. *Cell* 159: 487–498

Jia G, Fu YE, Zhao Xu, Dai Q, Zheng G, Yang Y, Yi C, Lindahl T, Pan T, Yang Y-G *et al* (2011) N6-methyladenosine in nuclear RNA is a major substrate of the obesity-associated FTO. *Nat Chem Biol* 7: 885–887

Jumaa H, Nielsen PJ (1997) The splicing factor SRp20 modifies splicing of its own mRNA and ASF/SF2 antagonizes this regulation. *EMBO J* 16: 5077–5085

Kawashima T, Douglass S, Gabunilas J, Pellegrini M, Chanfreau GF (2014) Widespread use of non-productive alternative splice sites in *Saccharomyces cerevisiae*. *PLoS Genet* 10: e1004249

Ke G, Meng Q, Finley T, Wang T, Chen W, Ma W, Ye Q, Liu T-Y (2017a) LightGBM: A highly efficient gradient boosting decision tree. *Adv Neural Inform Process Syst* 30: 3146–3154

Ke S, Pandya-Jones A, Saito Y, Fak JJ, Vagbo CB, Geula S, Hanna JH, Black DL, Darnell Jr JE, Darnell RB (2017b) m(6)A mRNA modifications are deposited in nascent pre-mRNA and are not required for splicing but do specify cytoplasmic turnover. *Genes Dev* 31: 990–1006

Kishor A, Fritz SE, Hogg JR (2019) Nonsense-mediated mRNA decay: the challenge of telling right from wrong in a complex transcriptome. *Wiley Interdiscip Rev RNA* 10: e1548

Kurosaki T, Popp MW, Maquat LE (2019) Quality and quantity control of gene expression by nonsense-mediated mRNA decay. *Nat Rev Mol Cell Biol* 20: 406–420

Kuroyanagi H, Ohno G, Mitani S, Hagiwara M (2007) The Fox-1 family and SUP-12 coordinately regulate tissue-specific alternative splicing *in vivo*. *Mol Cell Biol* 27: 8612–8621

Kuroyanagi H, Ohno G, Sakane H, Maruoka H, Hagiwara M (2010) Visualization and genetic analysis of alternative splicing regulation *in vivo* using fluorescence reporters in transgenic *Caenorhabditis elegans*. *Nat Protoc* 5: 1495–1517

Kuroyanagi H, Watanabe Y, Suzuki Y, Hagiwara M (2013) Position-dependent and neuron-specific splicing regulation by the CELF family RNA-binding protein UNC-75 in *Caenorhabditis elegans*. *Nucleic Acids Res* 41: 4015–4025

Langmead B, Salzberg SL (2012) Fast gapped-read alignment with Bowtie 2. *Nat Methods* 9: 357–359

Lareau LF, Brenner SE (2015) Regulation of splicing factors by alternative splicing and NMD is conserved between kingdoms yet evolutionarily flexible. *Mol Biol Evol* 32: 1072–1079

Lareau LF, Inada M, Green RE, Wengrod JC, Brenner SE (2007) Unproductive splicing of SR genes associated with highly conserved and ultraconserved DNA elements. *Nature* 446: 926–929

Lejeune F, Cavaloc Y, Stevenin J (2001) Alternative splicing of intron 3 of the serine/arginine-rich protein 9G8 gene. Identification of flanking exonic splicing enhancers and involvement of 9G8 as a trans-acting factor. *J Biol Chem* 276: 7850–7858

Lewis JA, Fleming JT (1995) Basic culture methods. In Epstein HF, Shakes DC (eds), *Caenorhabditis elegans: modern biological analysis of an organism*, Vol. 48, 1, pp 3–29. San Diego, CA: Academic Press

Li H (2018) Minimap2: pairwise alignment for nucleotide sequences. *Bioinformatics* 34: 3094–3100

Li Y, Na K, Lee HJ, Lee EY, Paik YK (2011) Contribution of *sams-1* and *pmt-1* to lipid homoeostasis in adult *Caenorhabditis elegans*. *J Biochem* 149: 529–538

Liberman N, O'Brown ZK, Earl AS, Boulias K, Gerashchenko MV, Wang SY, Fritsche C, Fady PE, Dong A, Gladyshev VN *et al* (2020) N6-adenosine methylation of ribosomal RNA affects lipid oxidation and stress resistance. *Sci Adv* 6: eaaz4370

Linder B, Grozhik AV, Olarerin-George AO, Meydan C, Mason CE, Jaffrey SR (2015) Single-nucleotide-resolution mapping of m6A and m6Am throughout the transcriptome. *Nat Methods* 12: 767–772

Liu H, Begik O, Lucas MC, Ramirez JM, Mason CE, Wiener D, Schwartz S, Mattick JS, Smith MA, Novoa EM (2019) Accurate detection of m(6)A RNA modifications in native RNA sequences. *Nat Commun* 10: 4079

Liu J, Yue Y, Han D, Wang X, Fu Y, Zhang L, Jia G, Yu M, Lu Z, Deng X *et al* (2014) A METTL3-METTL14 complex mediates mammalian nuclear RNA N6-adenosine methylation. *Nat Chem Biol* 10: 93–95

Liu N, Dai Q, Zheng G, He C, Parisien M, Pan T (2015) N^6-methyladenosine-dependent RNA structural switches regulate RNA-protein interactions. *Nature* 518: 560–564

Lombardini JB, Talalay P (1970) Formation, functions and regulatory importance of S-adenosyl-L-methionine. *Adv Enzyme Regul* 9: 349–384

Lorenz DA, Sathe S, Einstein JM, Yeo GW (2020) Direct RNA sequencing enables m⁶A detection in endogenous transcript isoforms at base-specific resolution. *RNA* 26: 19–28

Louloupi A, Ntini E, Conrad T, Orom UAV (2018) Transient N-6-methyladenosine transcriptome sequencing reveals a regulatory role of m6A in splicing efficiency. *Cell Rep* 23: 3429–3437

Luco RF, Pan Q, Tominaga K, Blencowe BJ, Pereira-Smith OM, Misteli T (2010) Regulation of alternative splicing by histone modifications. *Science* 327: 996–1000

Lun AT, Smyth GK (2016) csaw: a Bioconductor package for differential binding analysis of ChIP-seq data using sliding windows. *Nucleic Acids Res* 44: e45

McDaniel BA, Grundy FJ, Artsimovitch I, Henkin TM (2003) Transcription termination control of the S box system: direct measurement of S-adenosylmethionine by the leader RNA. *Proc Natl Acad Sci USA* 100: 3083–3088

McGlincy NJ, Tan LY, Paul N, Zavolan M, Lilley KS, Smith CW (2010) Expression proteomics of UPF1 knockdown in HeLa cells reveals autoregulation of hnRNP A2/B1 mediated by alternative splicing resulting in nonsense-mediated mRNA decay. *BMC Genom* 11: 565

McLuckey SA, Van Berkel GJ, Glish GL (1992) Tandem mass spectrometry of small, multiply charged oligonucleotides. *J Am Soc Mass Spectrom* 3: 60–70

Mendel M, Delaney K, Pandey RR, Chen KM, Wenda JM, Vagbo CB, Steiner FA, Homolka D, Pillai RS (2021) Splice site m(6)A methylation prevents binding of U2AF35 to inhibit RNA splicing. *Cell* 184: 1–18

Merendino L, Guth S, Bilbao D, Martinez C, Valcarcel J (1999) Inhibition of *msl-2* splicing by Sex-lethal reveals interaction between U2AF³⁵ and the 3' splice site AG. *Nature* 402: 838–841

Montange RK, Batey RT (2006) Structure of the S-adenosylmethionine riboswitch regulatory mRNA element. *Nature* 441: 1172–1175

Muir VS, Gasch AP, Anderson P (2018) The substrates of nonsense-mediated mRNA Decay in *Caenorhabditis elegans*. *G3* 8: 195–205

Ni JZ, Grate L, Donohue JP, Preston C, Nobida N, O'Brien G, Shiue L, Clark TA, Blume JE, Ares Jr M (2007) Ultraconserved elements are associated with homeostatic control of splicing regulators by alternative splicing and nonsense-mediated decay. *Genes Dev* 21: 708–718

Nilsen TW, Graveley BR (2010) Expansion of the eukaryotic proteome by alternative splicing. *Nature* 463: 457–463

Nishikawa K, Iwamoto Y, Kobayashi Y, Katsuoka F, Kawaguchi S-I, Tsujita T, Nakamura T, Kato S, Yamamoto M, Takayanagi H *et al* (2015) DNA methyltransferase 3a regulates osteoclast differentiation by coupling to an S-adenosylmethionine-producing metabolic pathway. *Nat Med* 21: 281–287

Obata F, Miura M (2015) Enhancing S-adenosyl-methionine catabolism extends *Drosophila* lifespan. *Nat Commun* 6: 8332

Parker MT, Knop K, Sherwood AV, Schurch NJ, Mackinnon K, Gould PD, Hall AJ, Barton GJ, Simpson GG (2020) Nanopore direct RNA sequencing maps the complexity of *Arabidopsis* mRNA processing and m6A modification. *Elife* 9: e49658

Pavlova N, Kaloudas D, Penchovsky R (2019) Riboswitch distribution, structure, and function in bacteria. *Gene* 708: 38–48

Pedregosa F, Varoquaux G, Gramfort A, Michel V, Thirion B, Grisel O, Blondel M, Prettenhofer P, Weiss R, Dubourg V *et al* (2011) Scikit-learn: machine learning in python. *J Mach Learn Res* 12: 2825–2830

Pendleton KE, Chen B, Liu K, Hunter OV, Xie Y, Tu BP, Conrad NK (2017) The U6 snRNA m⁶A Methyltransferase METTL16 regulates SAM synthetase intron retention. *Cell* 169: 824–835

Ping X-L, Sun B-F, Wang Lu, Xiao W, Yang X, Wang W-J, Adhikari S, Shi Y, Lv Y, Chen Y-S *et al* (2014) Mammalian WTAP is a regulatory subunit of the RNA N6-methyladenosine methyltransferase. *Cell Res* 24: 177–189

Pulak R, Anderson P (1993) mRNA surveillance by the *Caenorhabditis elegans smg* genes. *Genes Dev* 7: 1885–1897

Quinlan AR, Hall IM (2010) BEDTools: a flexible suite of utilities for comparing genomic features. *Bioinformatics* 26: 841–842

Ramani AK, Calarco JA, Pan Q, Mavandadi S, Wang Y, Nelson AC, Lee LJ, Morris Q, Blencowe BJ, Zhen M *et al* (2011) Genome-wide analysis of alternative splicing in *Caenorhabditis elegans*. *Genome Res* 21: 342–348

Ramani AK, Nelson AC, Kapranov P, Bell I, Gingeras TR, Fraser AG (2009) High resolution transcriptome maps for wild-type and nonsense-mediated decay-defective *Caenorhabditis elegans*. *Genome Biol* 10: R101

Roach NP, Sadowski N, Alessi AF, Timp W, Taylor J, Kim JK (2020) The full-length transcriptome of *C. elegans* using direct RNA sequencing. *Genome Res* 30: 299–312

Robinson JT, Thorvaldsdottir H, Winckler W, Guttman M, Lander ES, Getz G, Mesirov JP (2011) Integrative genomics viewer. *Nat Biotechnol* 29: 24–26

Roundtree IA, Luo G-Z, Zhang Z, Wang X, Zhou T, Cui Y, Sha J, Huang X, Guerrero L, Xie P *et al* (2017) YTHDC1 mediates nuclear export of N6-methyladenosine methylated mRNAs. *Elife* 6: e31311

Saint-Andre V, Batsche E, Rachez C, Muchardt C (2011) Histone H3 lysine 9 trimethylation and HP1γ favor inclusion of alternative exons. *Nat Struct Mol Biol* 18: 337–344

Schor IE, Rascovan N, Pelisch F, Allo M, Kornblihtt AR (2009) Neuronal cell depolarization induces intragenic chromatin modifications affecting NCAM alternative splicing. *Proc Natl Acad Sci USA* 106: 4325–4330

Schwartz S, Mumbach M, Jovanovic M, Wang T, Maciag K, Bushkin G, Mertins P, Ter-Ovanesyan D, Habib N, Cacchiarelli D *et al* (2014) Perturbation of m6A writers reveals two distinct classes of mRNA methylation at internal and 5' sites. *Cell Rep* 8: 284–296

Shi H, Wei J, He C (2019) Where, when, and how: context-dependent functions of RNA methylation writers, readers, and erasers. *Mol Cell* 74: 640–650

Shima H, Matsumoto M, Ishigami Y, Ebina M, Muto A, Sato Y, Kumagai S, Ochiai K, Suzuki T, Igarashi K (2017) S-adenosylmethionine synthesis is regulated by selective N^6-adenosine methylation and mRNA degradation involving METTL16 and YTHDC1. *Cell Rep* 21: 3354–3363

Shiraki N, Shiraki Y, Tsuyama T, Obata F, Miura M, Nagae G, Aburatani H, Kume K, Endo F, Kume S (2014) Methionine metabolism regulates maintenance and differentiation of human pluripotent stem cells. *Cell Metab* 19: 780–794

Sibley CR (2014) Regulation of gene expression through production of unstable mRNA isoforms. *Biochem Soc Trans* 42: 1196–1205

Son HG, Seo M, Ham S, Hwang W, Lee D, An SWA, Artan M, Seo K, Kaletsky R, Arey RN *et al* (2017) RNA surveillance via nonsense-mediated mRNA decay is crucial for longevity in *daf-2*/insulin/IGF-1 mutant *C. elegans*. *Nat Commun* 8: 14749

Sun Y, Bao Y, Han W, Song F, Shen X, Zhao J, Zuo Ji, Saffen D, Chen W, Wang Z *et al* (2017) Autoregulation of RBM10 and cross-regulation of RBM10/RBM5 via alternative splicing-coupled nonsense-mediated decay. *Nucleic Acids Res* 45: 8524–8540

Sureau A, Gattoni R, Dooghe Y, Stevenin J, Soret J (2001) SC35 autoregulates its expression by promoting splicing events that destabilize its mRNAs. *EMBO J* 20: 1785–1796

Tabrez SS, Sharma RD, Jain V, Siddiqui AA, Mukhopadhyay A (2017) Differential alternative splicing coupled to nonsense-mediated decay of mRNA ensures dietary restriction-induced longevity. *Nat Commun* 8: 306

Takei S, Togo-Ohno M, Suzuki Y, Kuroyanagi H (2016) Evolutionarily conserved autoregulation of alternative pre-mRNA splicing by ribosomal protein L10a. *Nucleic Acids Res* 44: 5585–5596

Tamiya H, Hirota K, Takahashi Y, Daitoku H, Kaneko Y, Sakuta G, Iizuka K, Watanabe S, Ishii N, Fukamizu A (2013) Conserved SAMS function in regulating egg-laying in *C. elegans*. *J Recept Sig Transd* 33: 56–62

Tourasse NJ, Millet JRM, Dupuy D (2017) Quantitative RNA-seq meta-analysis of alternative exon usage in *C. elegans*. *Genome Res* 27: 2120–2128

Turunen JJ, Verma B, Nyman TA, Frilander MJ (2013) HnRNPH1/H2, U1 snRNP, and U11 snRNP cooperate to regulate the stability of the U11–48K pre-mRNA. *RNA* 19: 380–389

Ule J, Blencowe BJ (2019) Alternative splicing regulatory networks: functions, mechanisms, and evolution. *Mol Cell* 76: 329–345

Walker A, Jacobs RL, Watts J, Rottiers V, Jiang K, Finnegan D, Shioda T, Hansen M, Yang F, Niebergall L et al (2011) A conserved SREBP-1/phosphatidylcholine feedback circuit regulates lipogenesis in metazoans. *Cell* 147: 840–852

Wang X, Zhao BS, Roundtree IA, Lu Z, Han D, Ma H, Weng X, Chen K, Shi H, He C (2015) N[6]-methyladenosine modulates messenger RNA translation efficiency. *Cell* 161: 1388–1399

Wani S, Kuroyanagi H (2017) An emerging model organism *Caenorhabditis elegans* for alternative pre-mRNA processing *in vivo*. *Wiley Interdiscip Rev RNA* 8: e1428

Webb B, Sali A (2016) Comparative protein structure modeling using MODELLER. *Curr Protoc Bioinformatics* 54: 5.6.1-5.6.37

Wei CM, Gershowitz A, Moss B (1975) Methylated nucleotides block 5' terminus of HeLa cell messenger RNA. *Cell* 4: 379–386

Winkler WC, Nahvi A, Sudarsan N, Barrick JE, Breaker RR (2003) An mRNA structure that controls gene expression by binding S-adenosylmethionine. *Nat Struct Biol* 10: 701–707

Wu S, Romfo CM, Nilsen TW, Green MR (1999) Functional recognition of the 3' splice site AG by the splicing factor U2AF[35]. *Nature* 402: 832–835

Xiao W, Adhikari S, Dahal U, Chen Y-S, Hao Y-J, Sun B-F, Sun H-Y, Li A, Ping X-L, Lai W-Y et al (2016) Nuclear m[6]A reader YTHDC1 regulates mRNA splicing. *Mol Cell* 61: 507–519

Yoshida H, Park S-Y, Oda T, Akiyoshi T, Sato M, Shirouzu M, Tsuda K, Kuwasako K, Unzai S, Muto Y et al (2015) A novel 3' splice site recognition by the two zinc fingers in the U2AF small subunit. *Genes Dev* 29: 1649–1660

Yoshida H, Park SY, Sakashita G, Nariai Y, Kuwasako K, Muto Y, Urano T, Obayashi E (2020) Elucidation of the aberrant 3' splice site selection by cancer-associated mutations on the U2AF1. *Nat Commun* 11: 4744

Zaccara S, Ries RJ, Jaffrey SR (2019) Reading, writing and erasing mRNA methylation. *Nat Rev Mol Cell Biol* 20: 608–624

Zheng G, Dahl J, Niu Y, Fedorcsak P, Huang C-M, Li C, Vågbø C, Shi Y, Wang W-L, Song S-H et al (2013) ALKBH5 is a mammalian RNA demethylase that impacts RNA metabolism and mouse fertility. *Mol Cell* 49: 18–29

Zhou KI, Shi H, Lyu R, Wylder AC, Matuszek Z, Pan JN, He C, Parisien M, Pan T (2019) Regulation of co-transcriptional pre-mRNA splicing by m[6]A through the low-complexity protein hnRNPG. *Mol Cell* 76: 70–81.e9

Zorio DA, Blumenthal T (1999) Both subunits of U2AF recognize the 3' splice site in *Caenorhabditis elegans*. *Nature* 402: 835–838